Internship Report

Of the Internship of Gerrald Gelderblom, student at

Twente University
Faculty of Engineering Technology
Laboratory of Thermal Engineering
Enschede, The Netherlands

Which is performed at

Universidad Nacional Autónoma de Mexico
Instituto de Investigaciones en Materiales
Departamento de Reología y Mecánica de Materiales
Mexico D.F., Mexico

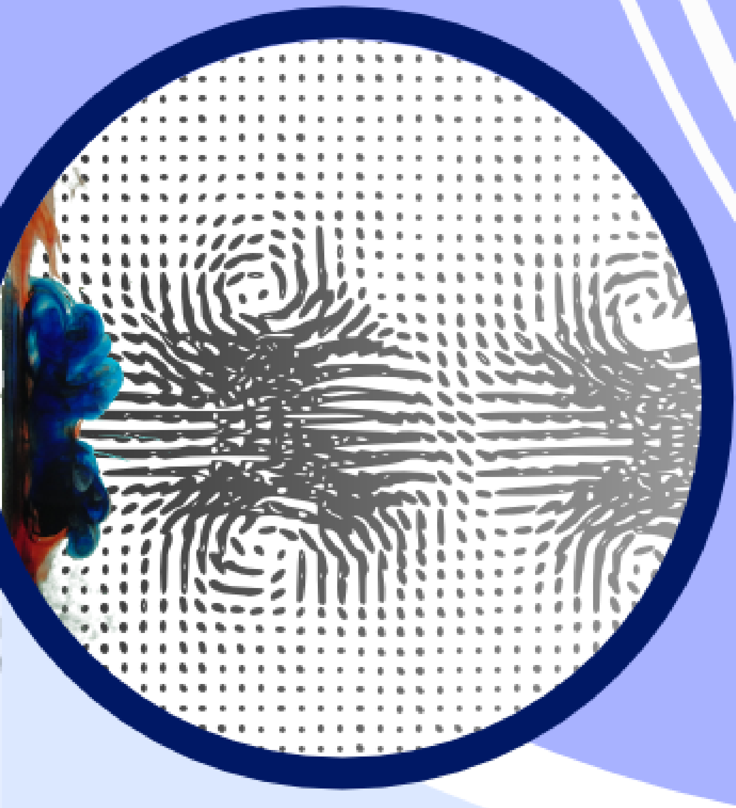

Head on Collision of a Vortex Ring and a Heated Wall

In the period of April 16, 2012 to July 31, 2012

Author: Gerrald Gelderblom
UT credential number s0158194

Professor UT: Prof. Dr. Ir. Th. Van der Meer
Professor UNAM: Prof. Dr. J. R. Zenit Camacho
Supervisor UNAM: Dr. Carlos Palacios
Internship coordinator: Dr. D. van der Belt

UNIVERSITY OF TWENTE.

Universidad Nacional Autónoma de México

PREFACE

6 years of study at the *University of Twente* almost brought me to starting my graduation project for my master Mechanical Engineering with the laboratory of Thermal engineering of Prof. Dr. Ir. Theo van der Meer. The last piece of work to be done before was an internship. My quest for a proper organization resulted in almost 4 months (April 13, 2012 to August 1, 2012) of internship in the amazing city Mexico D.F. Now 2 months after my return finally the tangible result of my work during this period is finished, and I am proud to present you the result!

Before the technical part begins, I want to seize the opportunity to thank certain people for their help and contribution. First I want to thank Professor Detlef Lohse from the group *Physics of Fluids* at the University of Twente for his help with finding this specific opportunity. Also thanks to Professor Roberto Zenit from the laboratory of *Reology and Fluid mechanics* at the *Universidad Nacional Autónoma de México* for offering me this internship, but also for the help, both professional and personal. Next I want to give my special thanks to Dr. Carlos (Charly) Palacios, for your supervision, tips, availability for questions and discussions and friendly intercourse. I'm looking forward to continue writing an article on the research we did! Finally, all the guys from the lab; It was great to be with you for those too short 3.5 months. I hope we have an opportunity to meet again, like I now do with Ernesto, while we live together in Hengelo.

Enjoy the report!

Date: / /

Gerrald Gelderblom

SUMMARY

This report deals with the process and results of an experimental research on the behavior of a vortex ring generated in water impinging a heated wall. This research is performed during an internship, part of the Thermal Engineering track of the master program of Mechanical Engineering at the University of Twente.

In the experiment, vortex rings were generated pushing a volume of water out of a tube into a basin. The vortex ring moves through the basin, ultimately colliding with a heated wall. The behavior was qualitatively studied using ink-visualizations and quantitatively investigated using PIV-measurements.

Vortex generation

The tube diameter has a diameter of 19.8mm. The piston was driven with a current of $[40\ 60\ 80]V$ for short periods of roughly $100 - 1000\ ms$, leading to a ratio between stroke and diameter of $R = [1\ 2\ 3\ 4]$. The piston velocity is calculated as the stroke divided by the time interval, and was determined to be between 7 and $23\ {}^{cm}/_{s}$. This is an average, the maximum is higher.

The range of Reynolds-numbers of the vortex rings depends on the definition of the Reynolds number. In a definition with the ring diameter as characteristic length and the vortex propagation velocity as characteristic velocity, the Reynolds number varies between 789 and 2770. The vortex diameter is between 30 and $35\ mm$, and the propagation velocity varies between 30 and $85\ {}^{mm}/_{s}$.

Boundary layer

The wall is heated using a thermal bath and a pump. Heating of the wall leads, due to buoyancy effects, to the formation of a natural convection flow along the wall. The experiment was performed for isothermal conditions and a wall temperature of $T = [0\ 40\ 55\ 70]°C$.

The Nusselt number for the heated cases varied between 150 and 210, indicating that convective heat transfer is dominant. The Prandtl number for the isothermal case is 6.22 while for a temperature of $70°C$ the Prandtl number is 4.17. The Grashof number is for all temperatures in the order of 10^8, indicating that the convection is still laminar, which is confirmed by the experiments. The Rayleigh number finally is in the order of 10^9, also indicating the dominance of convection.

Collision

For the isothermal case, it appeared that a transition in behavior appears for higher stroke ratio's (and circulation). For a stroke ratio up to $R = 1$, the ring diameter just increases. For a higher stroke ratio, boundary layer separation occurs, leading to the formation of a secondary or even tertiary ring. This ring moves around the primary ring. When it moves into the center of the primary ring, instability occurs, leading to break-up and reconnection into smaller rings.

For the heated cases, it appeared that the influence of the convection decreases for higher Reynolds numbers. The research focuses on the cases without boundary layer separation, in terms of conditions; the cases for $R = 1$. It is found that for this case, the top part of the ring moves closer to the wall than the bottom part. The radius of the top part decreases, while it increases for the bottom part. In contradiction to that, for the top part the circulation seems to 'dissipate' slower. The convection imposes swirl to the vertical side parts. These parts move up even faster than the horizontal top part, leading to a typical 'cat-head' shape.

TABLE OF CONTENTS

1 INTRODUCTION

This research is executed in 2012 by Gerrald Gelderblom at the laboratory of Rheology, institute of investigation on materials, part of the UNAM in Mexico. The aim of the research is to study the behavior of a vortex ring colliding with a heated wall.

1.1 Heat transfer enhancement

In the scientific area of heat transfer, a lot of research is done on the topic of heat transfer enhancement through so-called vortex promoters in heat-exchangers. These vortex promoters, which exist in many different shapes and configurations, usually generate vortices with their central axis in the direction of the flow and parallel to the wall. It is found that vortices contribute to heat transfer, but also generate resistance. Practically more energy is required for the transport of the transfer fluid.

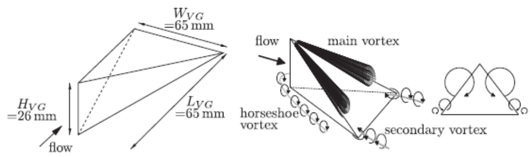

Picture 1-1 An example of a vortex promoter as studied by Henze, M. and Von Wolfersdorf, J. (2010) [8]

1.2 Vortex ring dynamics

In the scientific area of fluid mechanics, many researchers studied the dynamics of vortex rings. Vortex rings are donut-shaped vortical structures in fluids. They are often generated in nature and technology. Examples are vortex rings around rotors and in human hearts. Also in turbulent flows vortex rings are very common. As early as the year 1876, Helmholtz gave a first mathematical description of a vortex ring.

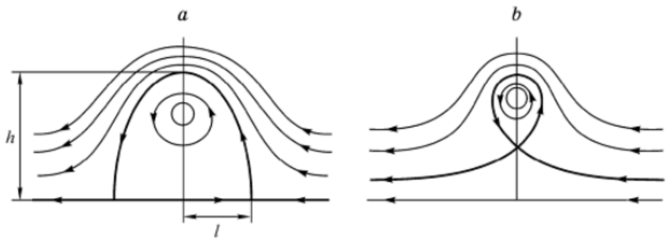

Picture 1-2 Streamlines in half of the section of a fat (a) or thin (b) version of Hill's Spherical Vortex, [10]

1.3 Research topic

To study the fundamental principles of heat transfer enhancement through vortices, an impinging vortex ring to a wall appears to be a very suitable experiment because they are easily reproduced and localized, which makes it easy to perform measurements. This research is based on and contributing to the work of Carlos Palacios and Roberto Zenit on respectively an experimental study on vortex ring dynamics and a numerical study on heat transfer enhancement due to vortex rings. The first aim of this research is not yet to study heat transfer, but the dynamics of the ring vortex approaching the wall and the heat-induced convection layer near the wall.

Because this report is an internship report, the language is quite descriptive and the format process-based. A more concise report is under preparation. Chapter 2 elaborates on the process of data collection. Chapters 3 and 4 deal with the characteristics of the vortex-ring and boundary layer, finally chapters 5 and 6 ultimately discuss the collision qualitatively and quantitatively.

2 Data collection

2.1 PIV data acquisition

The data used for analysis was collected using two PIV systems. A schematic representation of such a system is given in **Error! Reference source not found.**

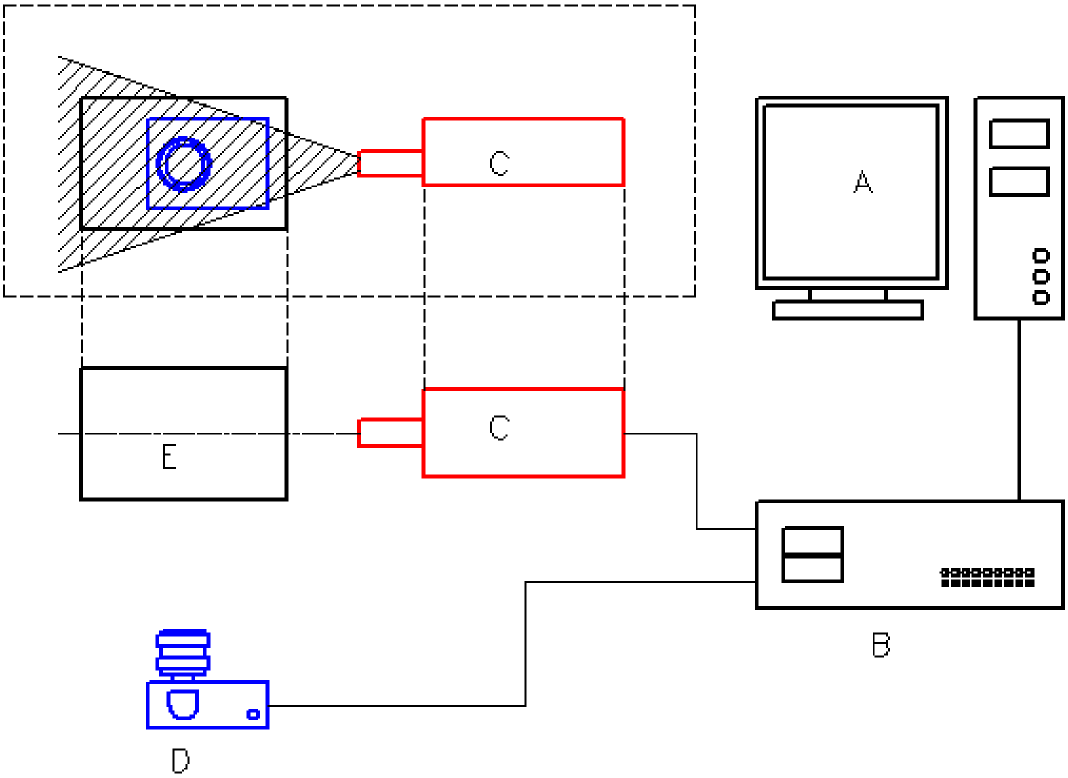

Picture 2-1 Schematic overview of PIV data acquisition system

The PIV system consists of a laser (C), a camera (D), a computer (A), a physical domain filled with water and hollow glass particles (E), a data buffer and a control unit for synchronization (B). Data is acquired using a pulsated laser which produces a 2D laser sheet. The laser sheet shines into the physical domain, where the particles (of neutral buoyancy) are illuminated. The camera makes pictures of the illuminated particles in the domain.

2.2 Ink visualizations

On top of PIV-measurements in a 2D vertical plane, also ink-visualisations were performed in order to acquire some tacit knowledge about the general behavior. The setup for these experiments is schematically drawn in Picture 2-2

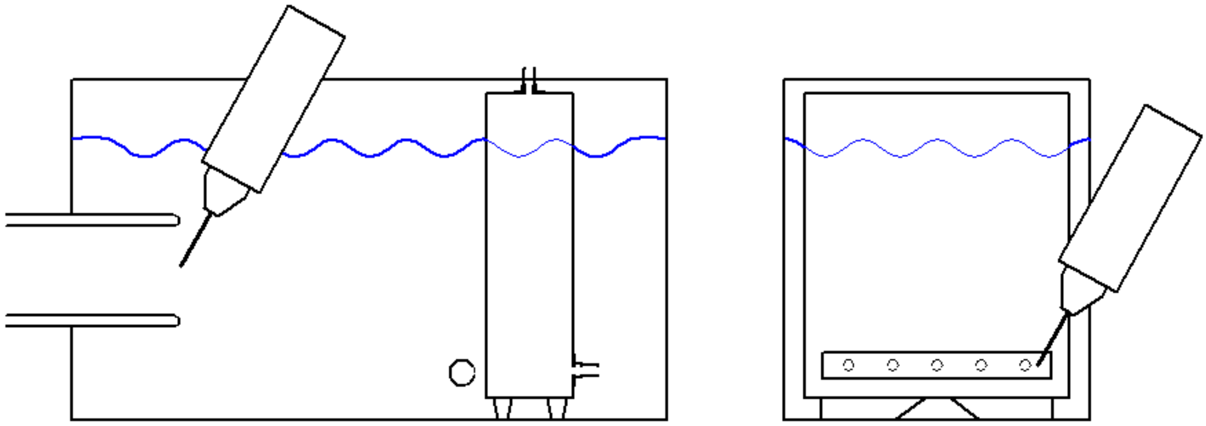

Picture 2-2 Schematic overview of ink injection

2.3 Vortex formation

The vortices were created using self-designed equipment, which is schematically represented in Picture 2-3

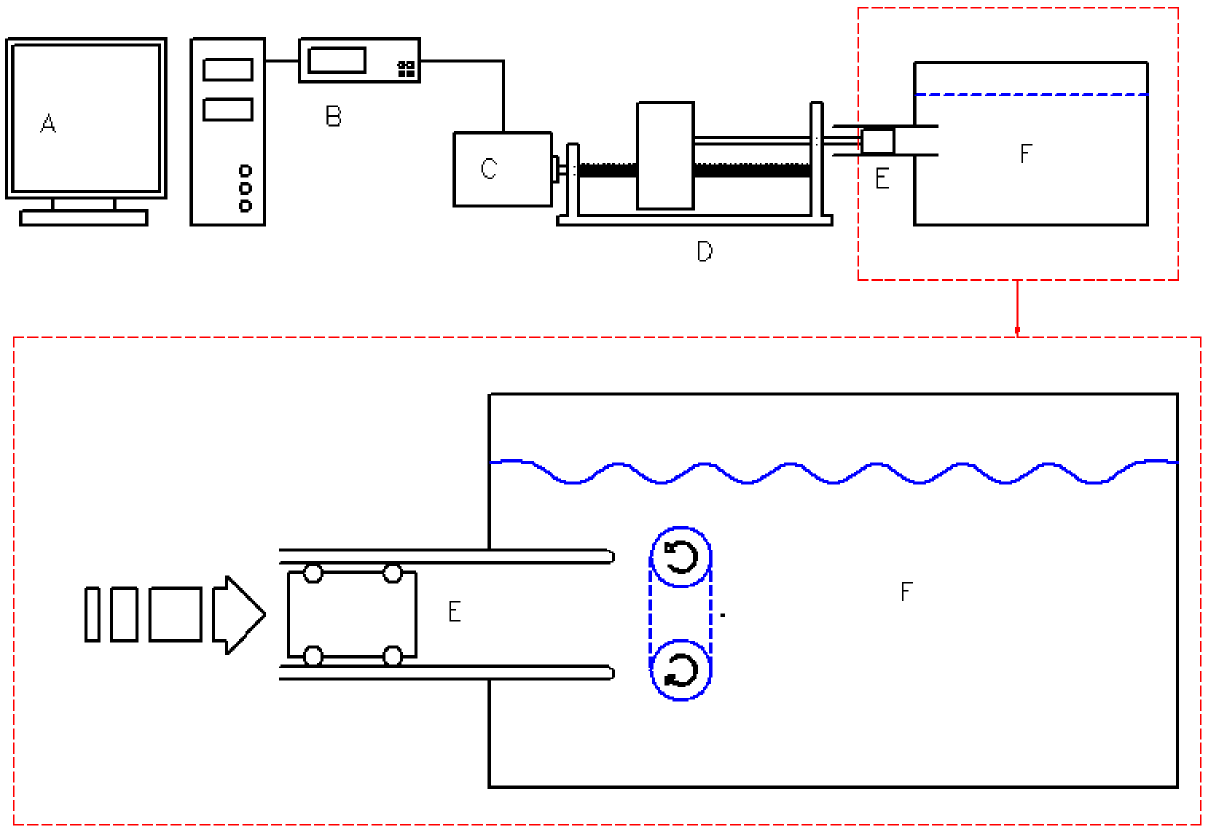

Picture 2-3 Schematic overview of vortex formation equipment

The vortex formation was realized by pushing a volume of fluid out of a round tube (E) with a free end in a bath filled with water (F). In the tube, a piston was free to move and push some fluid out of the tube. The piston was connected to a sledge (D) which was driven through a screw to a motor (C). The motor was driven by a power supply (B) controlled by the computer (A), where the voltage and time of exposure could be varied. The latter in order to produce vortex rings of different circulation, size and speed. Specifications of the equipment are given in Appendix A4. The tube diameter was

19,7mm, and one characterization of a certain experiment is to measure the stroke ratio, which was varied between 1 and 4.

2.4 Wall heating

The vortex rings are supposed to collide with a heated wall, which should be kept at a constant temperature. A schematic overview of the system used to realize this condition is given in Picture 2-4

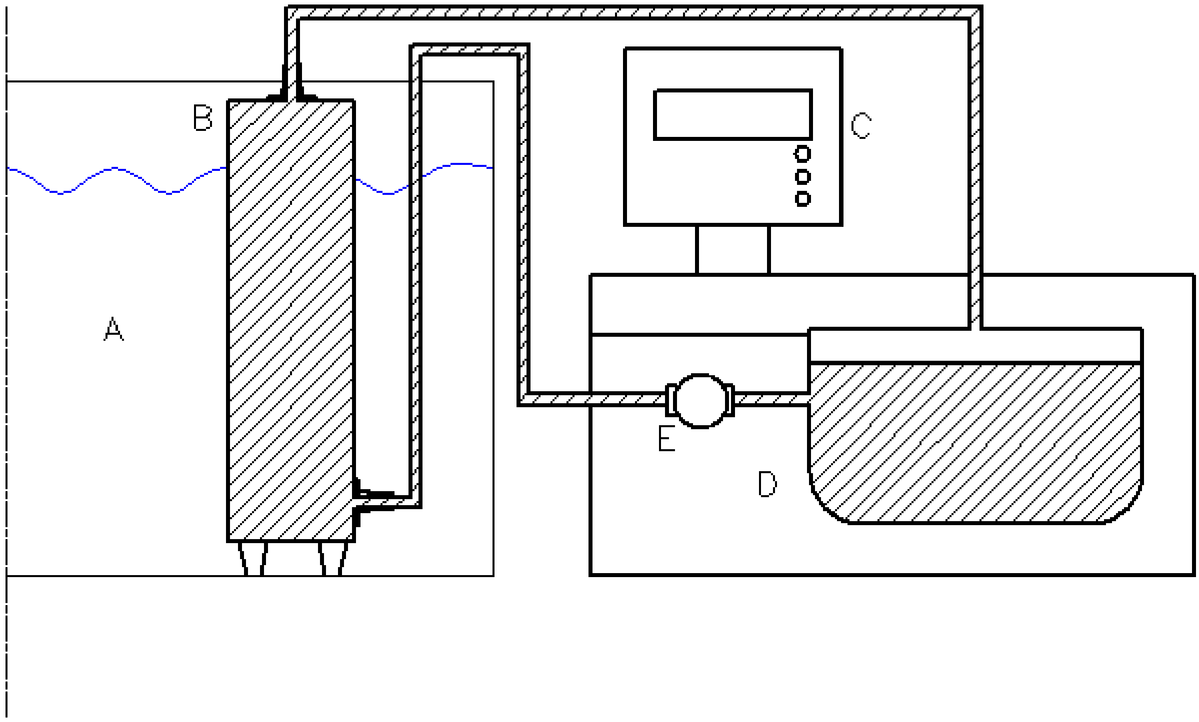

Picture 2-4 Schematic overview of wall and heating system

The temperature was heated using a thermal bath consisting of a water basin (D) with a pump (E) and a control unit (C) connected to a transparent hollow wall (B). This wall was placed in the water basin (A). Because the water inside the bath was kept at constant temperature, the temperature at the outside of the wall is more or less constant as well (approaching equilibrium). We had some problems with cracks due to thermal expension using a glass wall, so instead we used an acrylic wall. Unfortunately this wall was not completely flat, and also the thermal conductivity was one order of magnitude lower[1].

2.5 Basic Data Analysis

For examples in the description of the data analysis, an example experiment is used with a stroke ratio of 4 and a current of 80V.

Velocity

Starting from the pictures made by the camera, a velocity field in the form of a vector field is created using an cross-correlation toolbox included in the software of Dantec Dynamics (Both Flowmanager and Dynamic Studio).

A series of filters was applied to the results in order to remove noise in the vectormaps. These processes are (subsequently) peak validation, moving average and average filter. To avoid noisy results due to effects of example mirroring outside of the domain, the vectorfields were masked. For the autocorrelation, an overlap of 75% was used. The resolution of the direct vectorfields was either

[1] Acrylic glass: $0.19\ Wm^{-1}K^{-1}$, Glass: $1.2\ Wm^{-1}K^{-1}$

62×62 or 147×201, roughly covering an area of $0.16 \times 0.16\ m$ or $0.12 \times 0.18\ m$ Time resolution was, depending on the experiment, between 14Hz and 50Hz.

The result of this process is a velocity vector-map, of which a typical example is presented

This velocity vector-map gives an impression of velocities in a plane through the vortex-ring. From these velocities, other quantities can be calculated.

Vorticity

A first and important quantity is the vorticity, which can be calculated as the curl of the velocity

$$\vec{\omega} = \vec{\nabla} \times \vec{v}$$

This vorticity is highest in the strongest vortices. Though, the maximum vorticity doesn't occur at the center of the vortex ring, due to the contribution of the velocity gradient towards the middle of the ring-vortex.

A typical result of a vorticity field is given in Picture 2-6, in Picture 2-5 the maximum vorticity is marked, which shows that it doesn't correspond with the center of the vortex.

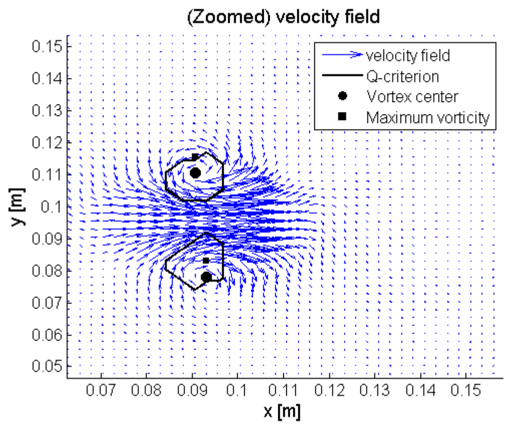

Picture 2-5 Velocity Vectorfield

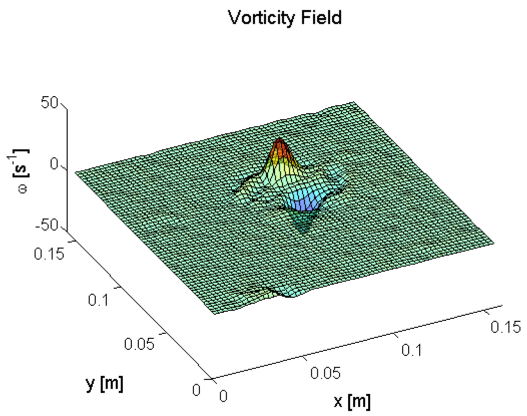

Picture 2-6 Vorticity Field

Circulation

Starting from the vorticity, it is easy to calculate the total circulation present in the vortex using

$$\Gamma = \int \omega dA$$

This is a 2D definition, though a vortex ring is a 3D entity. In literature, circulation is generic representated by the 2D circulation of just one section, while two of them are visible in one vectormap. On top of that, a proper method should be found to properly separate the vorticity of the vortex and the vorticity of the noise.

Q-criterion

The most general method to find the area of a vortex is the so-called Q-criterion [11]. The Q-criterion basically gives the ratio of rotation rate over strain rate. This means that Q>0 for a vortex, and Q<0 for shear flow.

The Q-criterion uses the decomposition of the velocity gradient in symmetric D and antisymmetric Ω components.

$$\nabla u = D + \Omega$$

Where $D = \frac{1}{2}\left((\nabla u) + (\nabla u)^t\right)$ and $\Omega = \frac{1}{2}\left((\nabla u) - (\nabla u)^t\right)$. D usually is called rate of strain vector, while Ω is referred to as the rate of rotation tensor.

The second invariant for incompressible flow ($\nabla u = 0$) is defined by

$$Q = \frac{1}{2}\left(|\Omega|^2 - |D|^2\right)$$

This definition is the Q-criterion, and can classify each point to be either in or outside the vortex. An example of such a Q-criterion map is presented in Picture 2-7

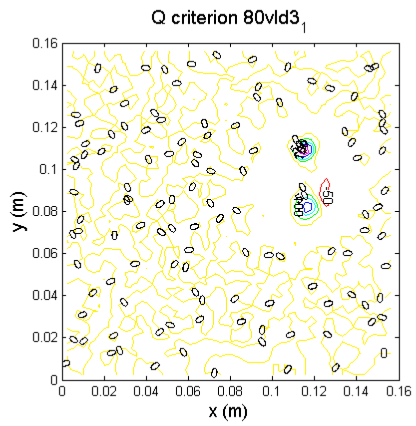

Picture 2-7 Q-criterion

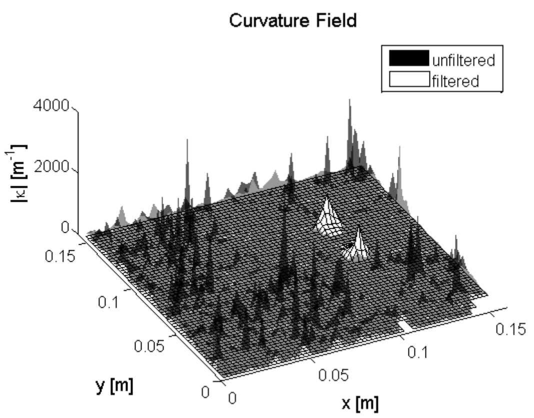

Picture 2-8 Absolute Curvature

Brown Curvature

A method to determine the position of the vortices is to determine the position of maximum curvature. One method to determine the curvature is named after Brown. Without elaborating on the concept behind the definition, just the definition is mentioned below.

$$K = \frac{1}{||u||^3}\left(v_x^2 \frac{\partial v_y}{\partial x} + v_x v_y \left(\frac{\partial v_y}{\partial y} - \frac{\partial v_x}{\partial x}\right) - v_y^2 \frac{\partial v_x}{\partial y}\right)$$

Where $||u||$ is the modulus of the velocity components;

$$||u|| = \sqrt{v_x^2 + v_y^2}$$

The absolute value of the curvature is presented in Picture 2-8. Peaks in the domain without a clear vortex are usually higher than the peaks for the vortex center. This indicates that filtering of the data is necessary. Here it can be seen that filtering of the curvature with the Q-criterion (in this case using a threshold of 8) here properly selects the peaks belonging to the vortices.

2.6 Vortex Tracking

Now since the basic field quantities are defined, they can be used to define the position of a vortex, ultimately in order to relate certain quantities to the vortex position rather than to the time after formation. The procedures are described in Appendix A6. Here just the selection of the method is justified.

Vortex tracking method selection

In many cases, determination of the vortex center gives the same result for both using normalized vorticity and curvature. A vortex center is always geometrically determined by 4 vectors around a center. It sometimes differs which one is selected. This might be arbitrary, but it has consequences for the measured velocity and diameter. In Picture 2-9 and Picture 2-10 a trajectory is plotted for both methods.

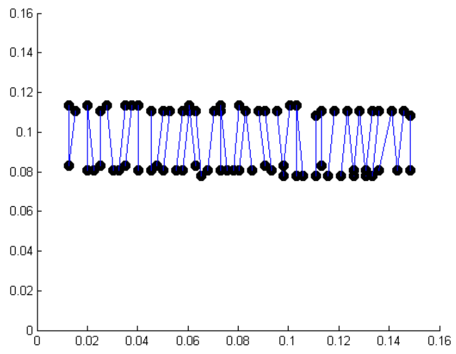

Picture 2-9 Vortex track based on curvature

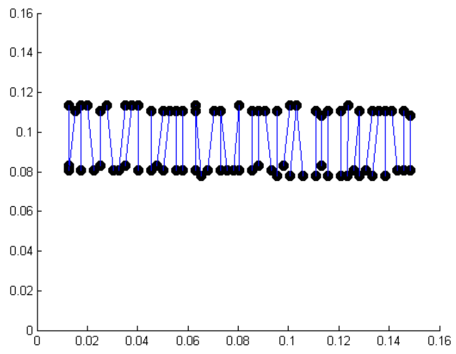

Picture 2-10 Vortex track based on normalized vorticity

Based on study of some of these tracks, the normalized vorticity method seems to give more homogeneous results. This is not based on a solid quantitative criterion.

3 Free moving vortex rings

Before the collision between a vortex ring and a wall was studied, first free moving vortex rings were studied. These experiments are performed in order to relate the settings of the equipment to the properties of the resulting vortex ring.

In the following graphs (Picture 3-1 to Picture 3-18), the circulation, propagation velocity and ring diameter are presented as functions of the vortex motor current and the stroke ratio $\left(\frac{L}{D_0}\right)$, where L is the stroke, and D_0 is the tube diameter.

Each of the quantities is made dimensionless using piston velocity v_p and tube diameter D_0. v_p is defined as $\frac{L_1 - L_0}{\Delta t}$. L_0 is the initial position, L_1 is the final position of the piston and Δt is the time interval in which the piston is moving. This means that v_p is actually the average piston velocity, the maximum is higher. It should be noticed that v_p is dependent on the settings of the experiment, while the tube diameter is independent of the settings of the experiment.

The data is extracted from 6 experiments for each combination of variables. 3 identical experiments for 2 camerapositions. The lines are averages, the errorbars are the maxima and minima for the three experiments at a certain vortex position. This means that it is not the standard deviation. The amount of experiments was not sufficient to determine a relevant standard deviation.

3.1 Vortex characteristic domains

First some relevant domains for parameters of the experiment are presented in Table 3-1, which are in fact averaged over three experiments. On top of this the Reynolds numbers are given. It should be noticed that different definitions of the Reynolds number are possible, and also used in literature.

For Reynolds number, the following definitions are used:

$$Re_1 = \frac{v_p D_0}{\nu}, Re_2 = \frac{v_p R}{\nu}, Re_3 = \frac{U_v D_v}{\nu}$$

In which v_p is the piston velocity, D_0 is the tube diameter R is the stroke ratio, U_v is the vortex speed and D_v is the vortex diameter.

V	R	Re_1	Re_2	Re_3	$U_v * 10^{-3}$	$D_v * 10^{-3}$
80	**4**	3214	12617	2770	83.71	34.01
	3	3183	10226	2354	74.13	32.79
	2	3004	6322	1395	52.01	31.11
60	**4**	2487	10022	2253	66.39	35.08
	3	2468	7485	1819	59.26	32.71
	2	2487	5130	1244	47.00	30.81
40	**4**	1537	6179	1332	43.24	34.31
	3	1550	4819	1126	38.13	33.86
	2	1586	3176	789	32.19	31.64

Table 3-1 Vortex characteristic domains

3.2 Circulation

In Picture 3-1 to Picture 3-6 the (dimensionless) circulation is presented as distributed over the position of the ring. What we can notice first is that we can find a transient formation period, which is dependent to the stroke ratio. For higher stroke ratio it takes longer before we find a maximum in the circulation, which is an indication of the position where the vortex ring is fully developed.

We can see a more than proportional relation between the stroke ratio and the dimensionless circulation present in the vortex ring. It is possible that it scales using vortex speed rather than piston velocity, but this is still about to be analyzed.

The influence of impulse (through voltage) on circulation scales proportionally with the piston velocity, this means that increasing the impulse also increases the circulation.

After the vortex is fully formed, the circulation decreases slowly, this is expected due to losses caused by dissipation.

3.3 Ring Diameter

In Picture 3-7 to Picture 3-12 the (dimensionless) ring diameter as distributed over the position is presented. The errors are relatively high, this is caused by the resolution. Of course this influence is smaller for larger ring-radii. For a typical ring diameter of 3 cm and a resolution of 0.25mm, one pixel difference already means 8.4% variation. For this reason the errorbars are only presented for the middle images, just to give an impression of the size of the errorbars.

We can see that increasing the stroke ratio results in a bigger ring, while increasing the impuls (through voltage) doesn't make a significant difference. After the vortex is fully formed, the ring diameter increases slowly.

3.4 Ring Velocity

In Picture 3-13 to Picture 3-18 finally (dimensionless) velocity is presented. The errors are relatively high, this is caused by the resolution. Again the errorbars are just presented for the middle figures.

We can see a more than proportional relation between the stroke ratio and the (dimensionless) ring velocity. The ring velocity scales proportionally with the piston velocity.

After the vortex is fully formed, the ring speed decreases slowly.

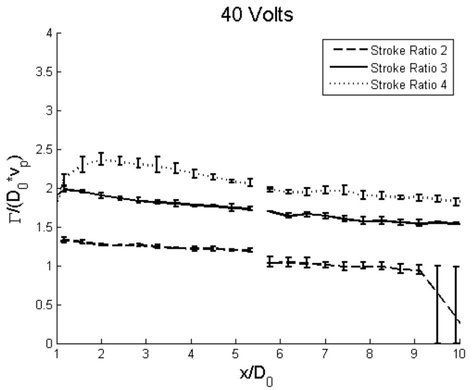

Picture 3-1 Circulation as function of Stroke Ratio

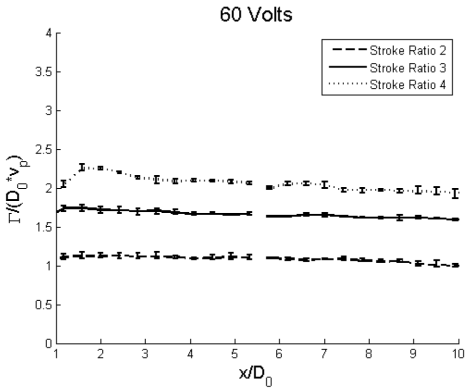

Picture 3-2

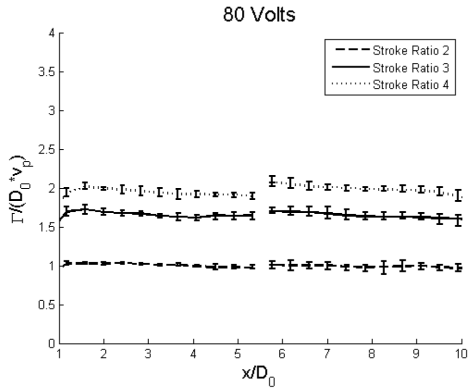

Picture 3-3

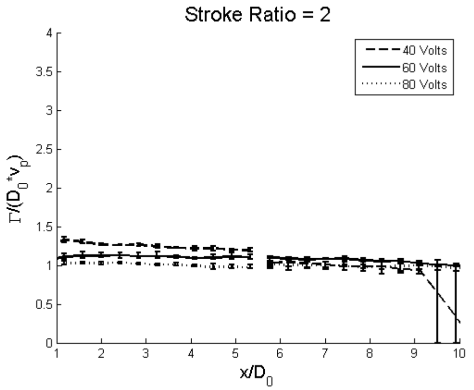

Picture 3-4 Circulation as function of Voltage

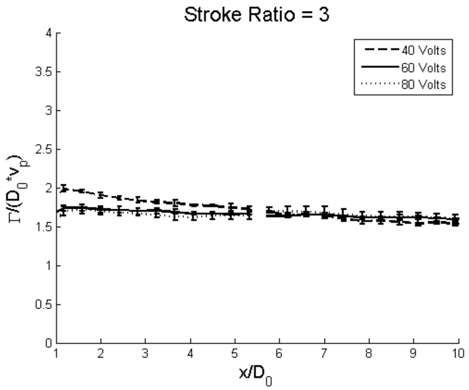

Picture 3-5

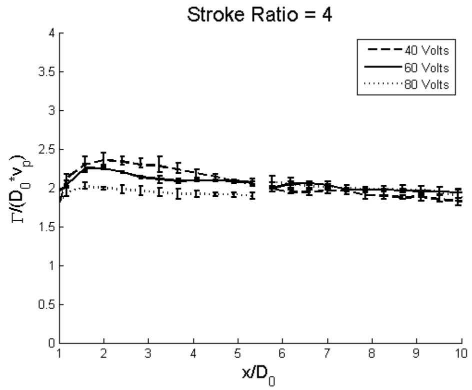

Picture 3-6

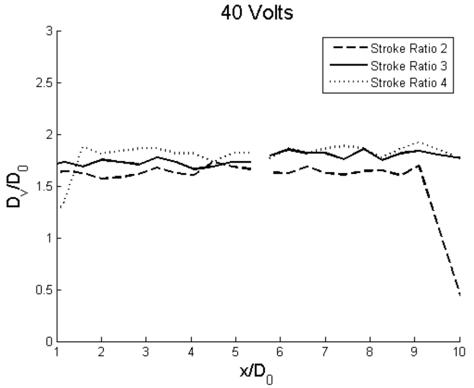

Picture 3-7 Ring diameter as function of Stroke Ratio

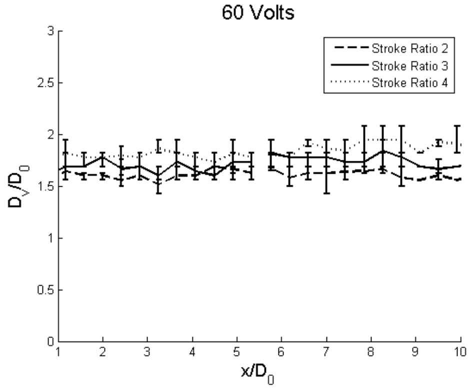

Picture 3-8

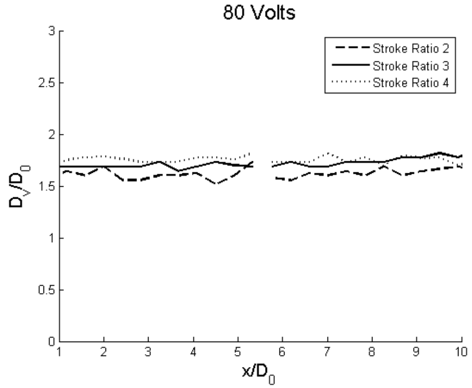

Picture 3-9

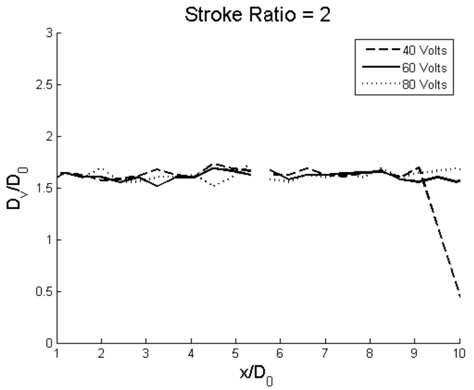

Picture 3-10 Ring diameter as function of Voltage

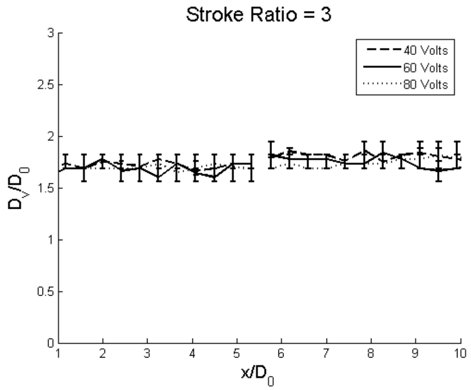

Picture 3-11

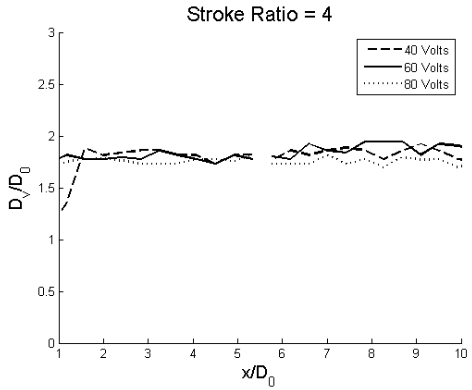

Picture 3-12

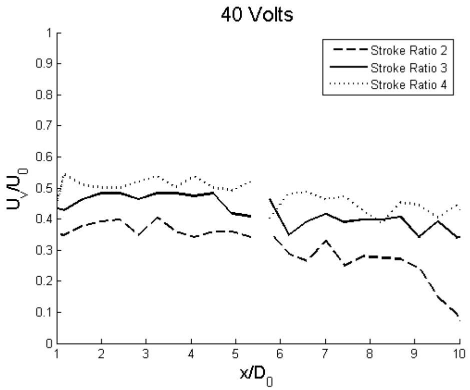

Picture 3-13 Ring velocity as function of Stroke Ratio

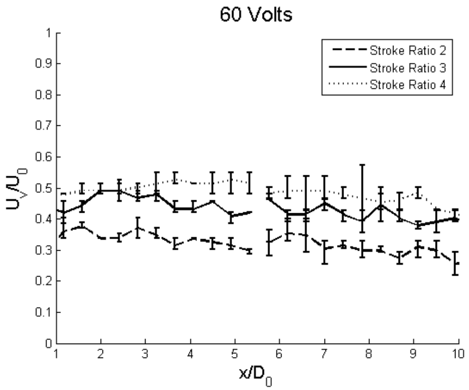

Picture 3-14

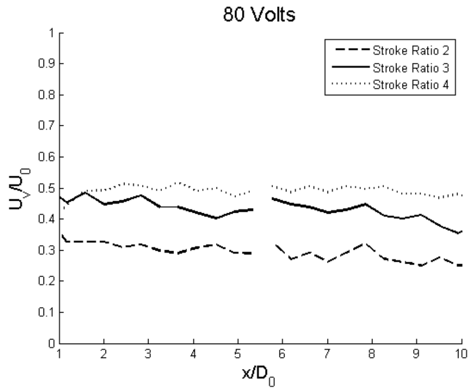

Picture 3-15

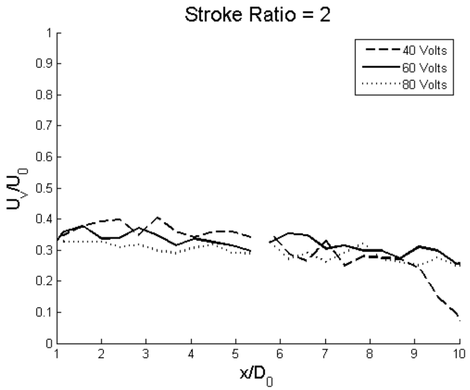

Picture 3-16 Ring velocity as function of Voltage

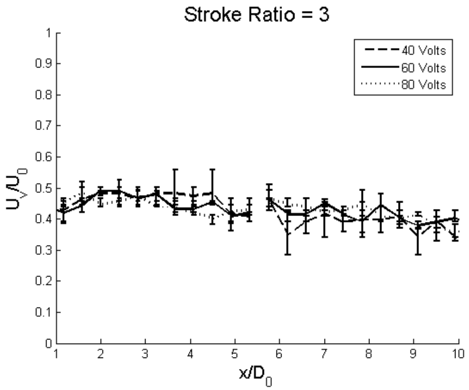

Picture 3-17

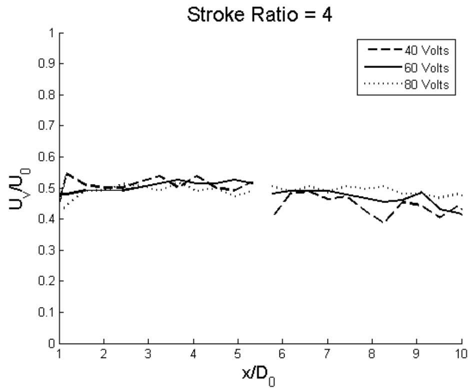

Picture 3-18

4 Boundary layer development and classification

For the classification of the boundary layer, 6 experiments were performed. The wall was heated up to 40°C, 55°C or 70°C and placed in the bath. After that each 15 seconds 4 images were made using the PIV-system. It is expected that because the wall is added to the bath first a lot of disturbance will be present which will dissipate slowly. Due to the heated wall, there will develop an equilibrium with a convective flow along the wall and a feedback flow through the tank.

First the velocity profiles through the tank are investigated. In this report just an example is shown for the moment usually the experiment is performed (2,5 minutes after adding the wall to the bath). For each temperature 2 profiles are presented, which are for both experiments performed for each temperature. An average doesn't make sense because the exact configuration has a large statistic variation and 2 experiments is not enough to determine a statistic average.

4.1 Boundary Layer characteristic domain

The domains for some different dimensionless numbers are given in Table 4-1.

	$\Delta T = 0$	$\Delta T = 20$	$\Delta T = 35$	$\Delta T = 50$
Grashof	0	$1.73 * 10^8$	$3.03 * 10^8$	$4.33 * 10^8$
Prandtl	6.22			4.17
Nusselt	0.68	155.01	184.60	206.45
Rayleigh	0	$1.08 * 10^9$	$1.88 * 10^9$	$2.69 * 10^9$

Table 4-1 Boundary Layer characteristic domains

4.2 Characteristics of the flow in the domain

Below some images are printed which give an overview of the flow pattern present in the basin. They are printed for different times so the development can qualitatively be extracted.

First the average of the vertical velocity is plotted as function of the horizontal position (Picture 4-1) and the average of the horizontal velocity is plotted as function of the vertical position (Picture 4-2). For the vertical velocity we see a boundary-layer which is stable but the velocity decreases. For the horizontal velocity generally it is found that the velocity is positive at the top of the bath, and negative at the bottom of the bath. At the top, higher velocities are found. Reason might be that here is a surface with air, and the images of the camera are not made at the vertical middle of the basin. Under the tube (and the middle of the images) is more water than above.

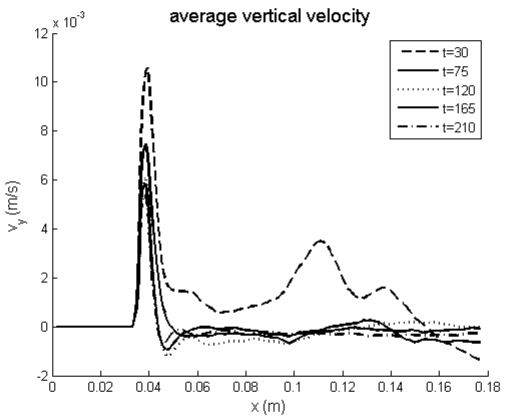

Picture 4-1 Average vertical velocity BL

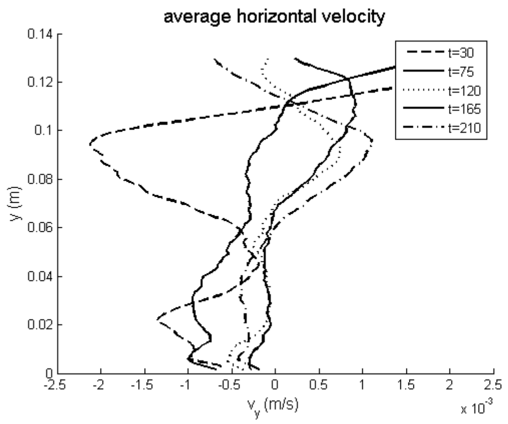

Picture 4-2 Average horizontal velocity BL

Now the maximum vertical position is plotted as function of the y-axis in Picture 4-3, and the position of this maximum vertical position is represented in Picture 4-4. The large variations in the vertical velocity are caused by the turbulent nature of the boundary layer. The outlier in the position near the bottom of the picture is caused by the fact that the flow near the wall is masked for the first $\pm$ 0.5 cm, which makes it impossible to find the real position. The boundary of the mask is indicated by the fat blue line.

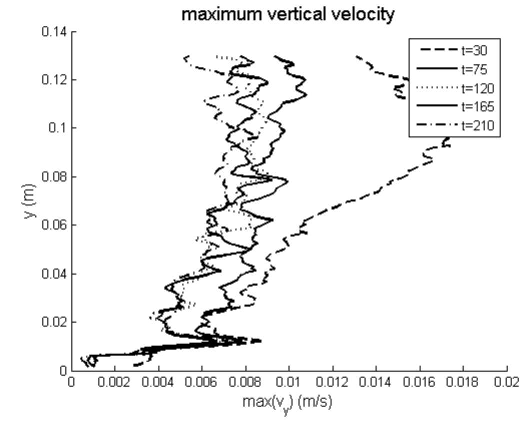

Picture 4-3 Maximum vertical velocity BL

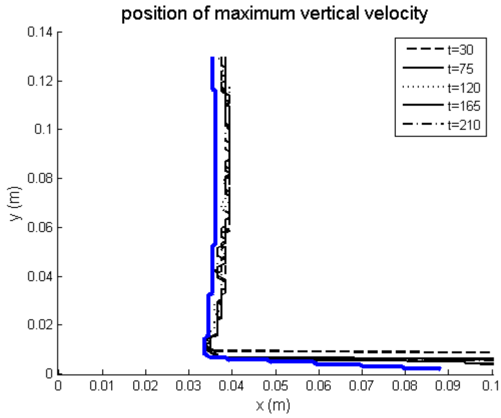

Picture 4-4 Boundary Layer geometry

4.3 Development of the boundary layer

Now the development of the boundary layer velocity is represented in time. For the first plot (Picture 4-5) first is for each vertical row the average determined, while thereafter the maximum value is extracted. This value is logically at the center of the boundary layer. The second graph (Picture 4-6) is produced the other way round, first the maximum velocity is calculated for each horizontal array of values, which is subsequently averaged over the y-axis. The results are, as expected, comparable.

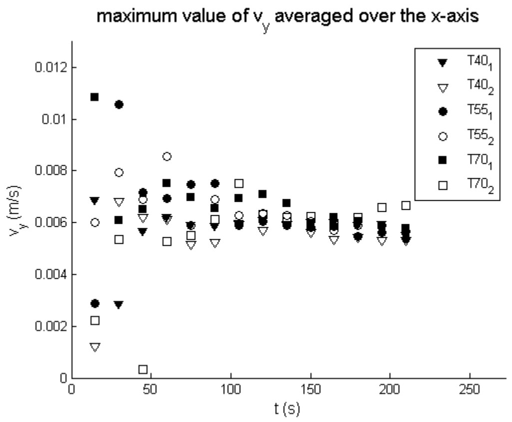

Picture 4-5 Vertical velocity of BL (1)

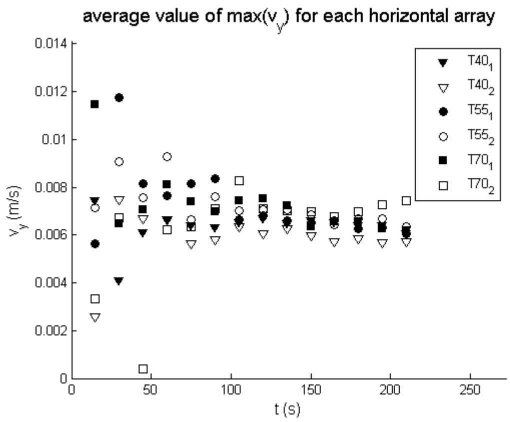

Picture 4-6 Vertical velocity of BL (2)

From this picture we can find (except for $T70_2$) first a lot of noise due to adding the wall, and after that a (probably linearly) decreasing boundary layer velocity. This boundary layer is probably decreasing because for the equilibrium position there is a large temperature gradient trough the glass wall, which makes the actual wall temperature much lower than the original temperature. As expected for higher temperatures the velocity seems to be little higher.

4.4 Circulation evaluation

Now the evaluation of the circulation in the domain is investigated. In Picture 4-7 the circulation is calculated for just the whole domain. Secondly, in Picture 4-8, the circulation is calculated for the absolute values of the vorticity.

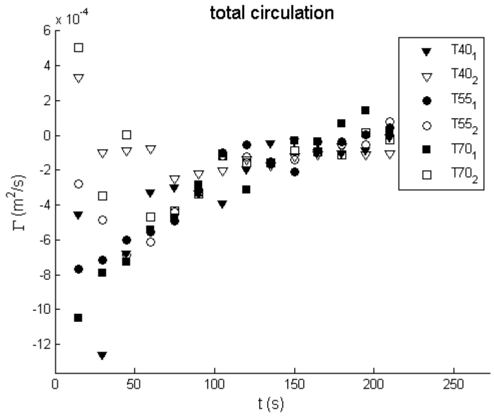

Picture 4-7 Regular circulation total domain

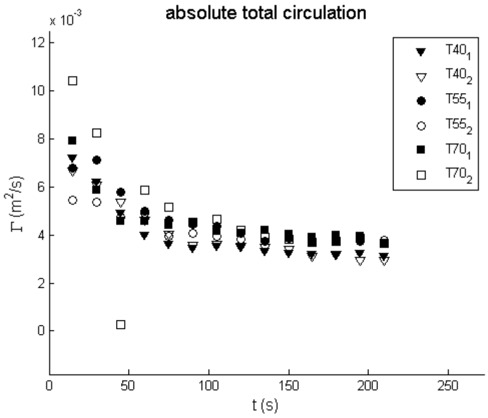

Picture 4-8 Absolute circulation total domain

In Picture 4-7 initially first a lot of noise is present. This is caused by the 3D nature of the motion in the domain. After that the circulation increases. This is caused by the fact that the boundary layer effectuates a 'convection role' with positive vorticity. This role is continuously fed by the energy from the wall, which makes that the circulation increases. In order to study the real 'amount of vorticity' also the absolute vorticity is integrated, which shows in Picture 4-8 a decrease which seems to obey a power law. The negative tendency of this circulation is expected. First the circulation due to disturbance dissipates, and after that also the boundary layer becomes weaker as we have seen in Picture 4-1and Picture 4-2.

Next the circulation is determined for 2 relevant part of the domain, first the part where the vortex ring moves. In this part we need low circulation (and low velocities). The second selection contains the part where the boundary layer is. For an indication of the areas used, see Picture 4-9 below.

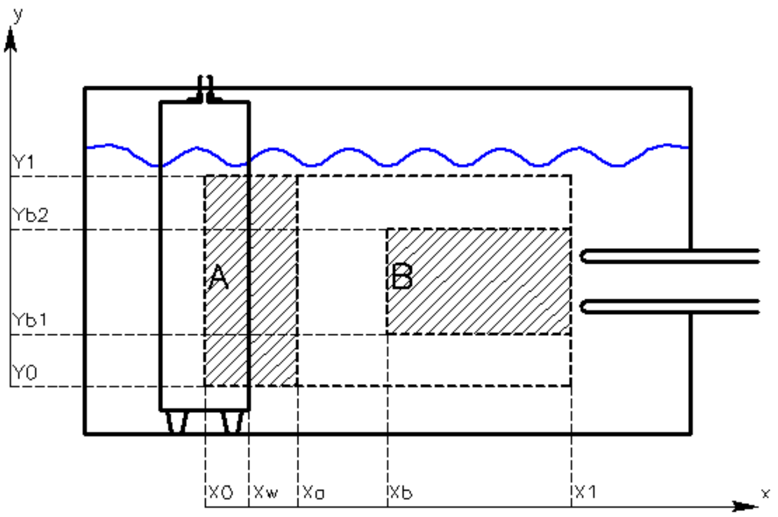

Picture 4-9 Area selections

x_0	0
x_1	0.177
x_w	± 0.035
x_a	0.442
x_b	0.085
y_0	0
y_1	0.1297
y_b1	0.0324
y_b2	0.0972

Table 4-2 Selection dimensions

First the part indicated with an A in Picture 4-9 is studied. The circulation and 'absolute circulation' for this part are given in Picture 4-10 and Picture 4-11.

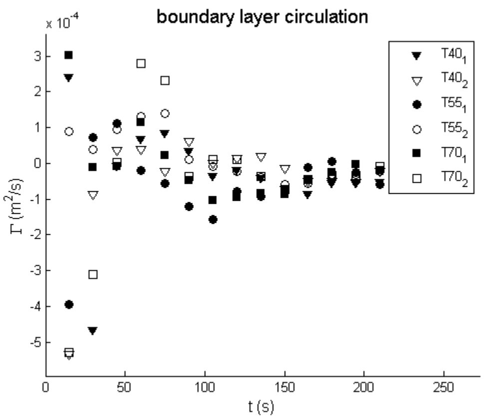

Picture 4-10 Regular circulation BL

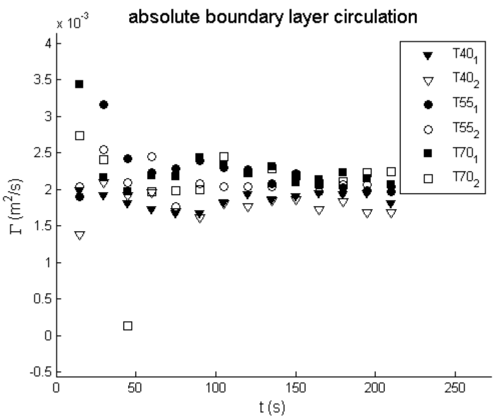

Picture 4-11 Absolute circulation BL

Looking at Picture 4-10 we can find again some noise first, which decreases. After that the circulation increases for a while but seems to find a maximum. Combined with Picture 4-11 for the absolute circulation which seems to follow quite different paths for different experiments, we conclude that the initial disturbance induced by placing the wall dissipates, or (depending on the nature of the disturbance present) contributes (partially) to the convection role which is found in equilibrium position.

Now finally we look at the region indicated with B in Picture 4-9, the circulation and partial circulation are presented in Picture 4-12 and Picture 4-13.

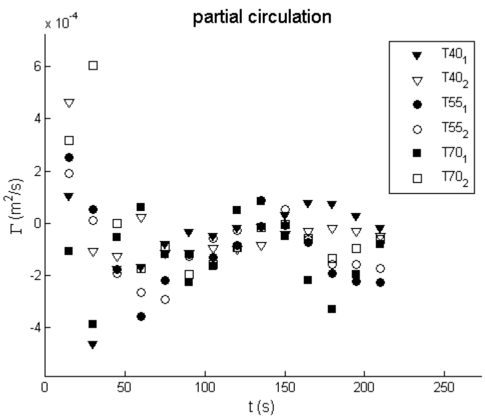

Picture 4-12 Regular circulation vortex trajectory

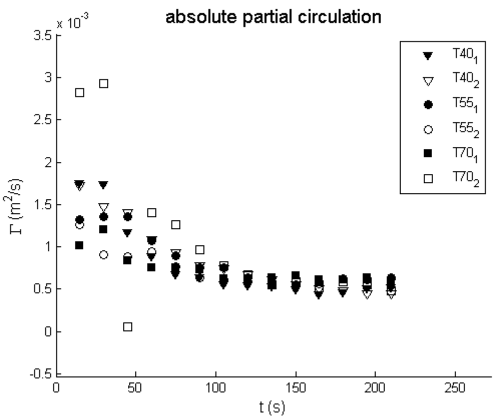

Picture 4-13 Absolute circulation vortex trajectory

It is beyond the scope of this research to explain the minimum and maximum, it can be interesting for further research. Here we find most important that the circulation is quite low and that it stabilizes after about 150 seconds.

In Picture 4-14Picture 4-14, for one temperature the absolute circulation plots are weighted by the area used to calculate them. It can be seen that the boundary layer has the highest circulation, and the average for the whole domain is higher than the part where the vortex ring will propagate. The second Picture 4-15 gives a velocity map with the partial areas indicated.

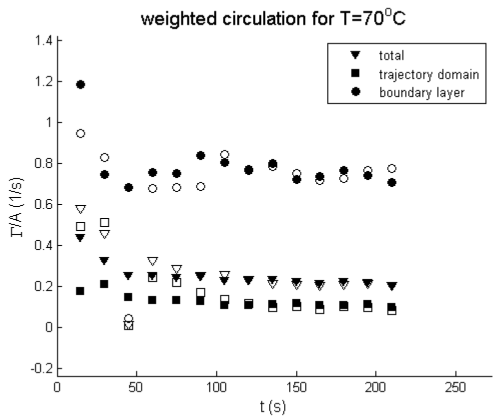

Picture 4-14 Weighted circulation

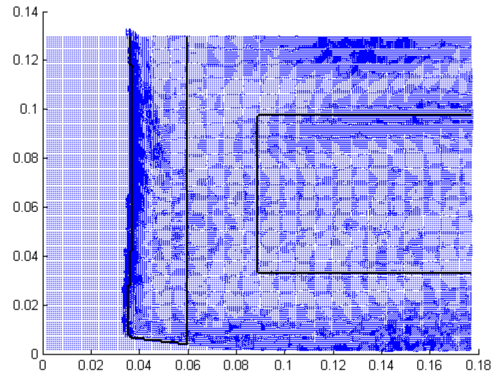

Picture 4-15 Selected areas

5 QUALITATIVE COLLISION BEHAVIOR

In order to study the general behavior of the collision, a 2D potential flow model was constructed and some ink experiments were performed.

5.1 2D potential flow

First of all it should be noticed that the flow is not 2D and not potential, which is quite a serious remark for the results of such a 2D potential flow model.

The model is made by a starting position of a vortex pair of unequal strength, close to a wall (modeled by the image) and a shear flow (modeled by an array of vortices), see Picture 5-1. The impact of each of these conditions is examined separately.

In **Error! Reference source not found.** also the forces are presented who act to the vortices. The forces A and B are caused by the difference in strength. The forces C and D are caused by the shear flow, the forces E and F are caused by the mirrors. The forces to the left (also caused by the mirrors) are left out in this balance. It can be expected that the top vortex will move towards the wall and upward, and the bottom vortex moves not as far to the wall, and maybe even backward to the wall due to the force caused by the strength difference. The vortex will move either upward or downward depending on the strength of the shear flow compared to the strength of the vortex.

First the collision of a vortex pair with a wall is considered. A wall is simulated with the image of the vortex at an equal distance at the other side of the wall. The effect is that the vortex slows down and the distance between the vortices increases, see Picture 5-2.

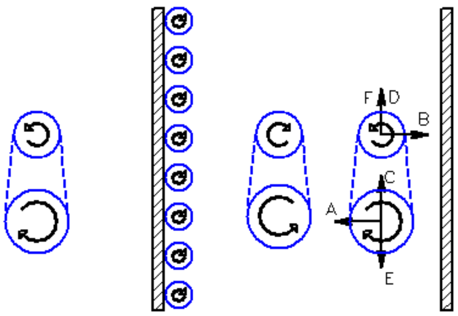

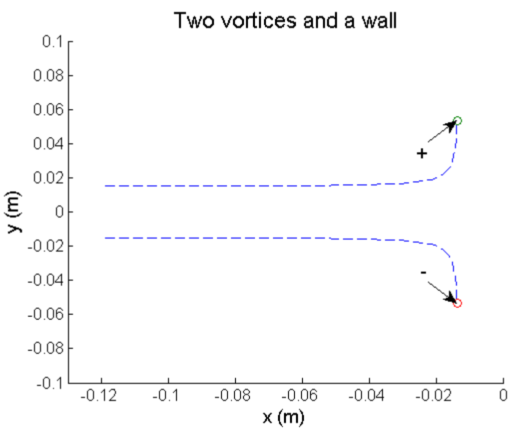

Picture 5-1 Flow model and Free Body Diagram

Picture 5-2 Standard 2D potential flow collision

Second the interaction of a vortex pair with a shear flow is considered. It is found that a shear flow causes just a vertical movement of the vortex (Picture 5-3). Finally, it is found that there is some vorticity transport. In the end the bottom vortex appears to be stronger than the one at the bottom. Such a pair of unequal strength is considered in Picture 5-4. It can be seen that the trajectory 'bends' in the direction of the stronger vortex.

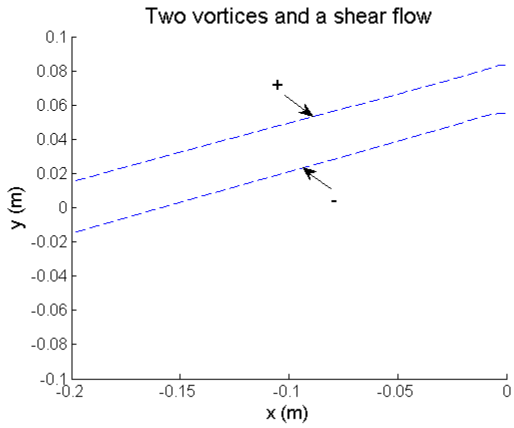

Picture 5-3 2D potential flow shear interaction

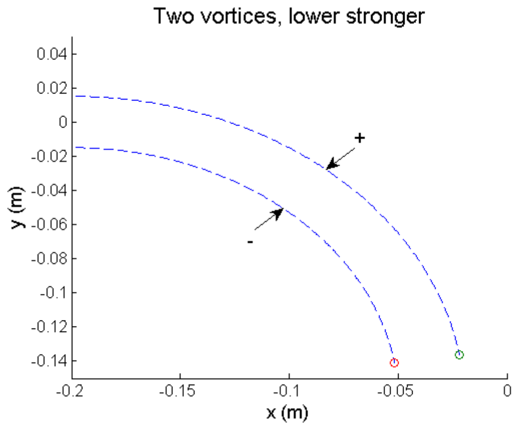

Picture 5-4 2D potential flow unequal vortex interaction

Now finally all effects are combined. The velocity field is given in Picture 5-5. The trajectory that follows from this situation is given in Picture 5-6. This trajectory is qualitatively comparable to the trajectory found in the experiments.

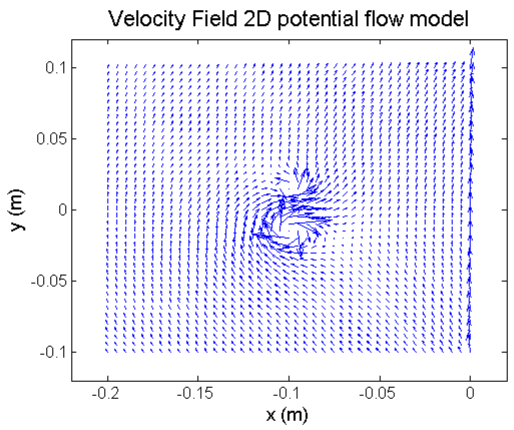

Picture 5-5 Velocity map 2D potential flow model

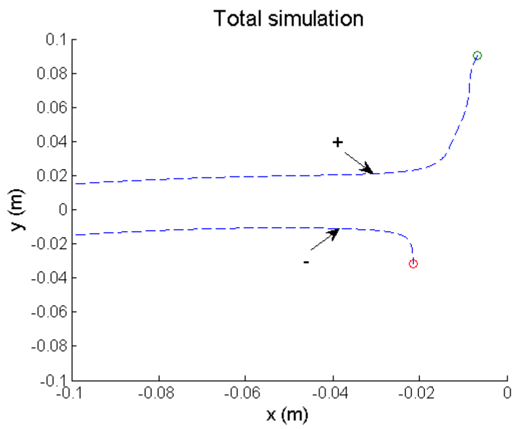

Picture 5-6 Trajectory full 2D potential flow model

5.2 Ink visualizations

The camera was placed either placed coaxial to the tube or perpendicular to the tube. Ink experiments were performed for the temperature differences $\Delta T = [0\ 35\ 50]$ and stroke ratio $R = [1\ 2]$.

Ultimately there should be a $t = 0$ position for all experiments which would make it possible to compare developments in time. Unfortunately it was not possible to determine this accurate enough. The time between frames is equal for all experiments, but it is possible that there is a lag between the top and bottom picture for both experiments.

For the isothermal case the results are printed in Picture 5-7 and Picture 5-8. This behavior is thoroughly described by Arévalo, Hernândez, Nicot and Plaza [5], [7] and Doligalski, Smith and Walker [1], [2]. The results are in agreement.

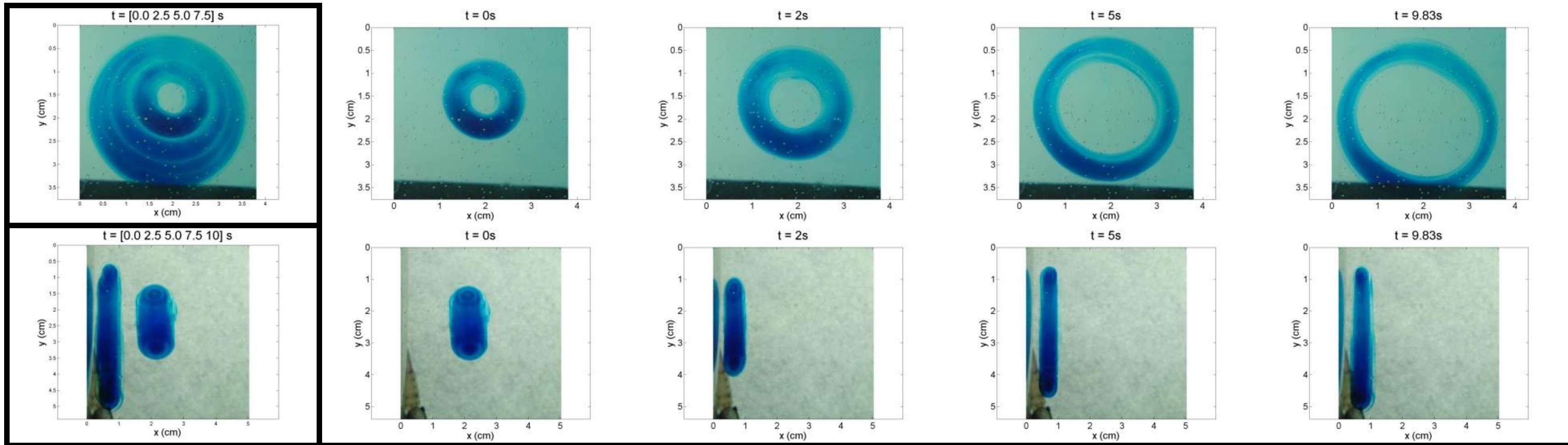

Picture 5-7 Ink visualizations $\Delta T = 0, R = 1$

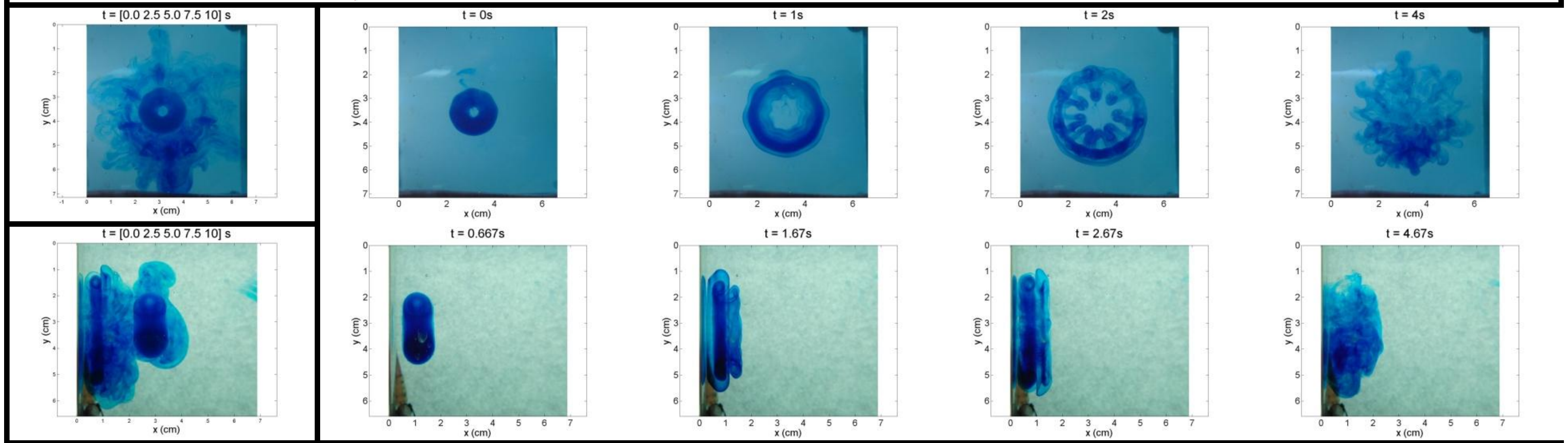

Picture 5-8 Ink visualizations $\Delta T = 0, R = 2$

The same experiment is performed with temperature differences, in Picture 5-9 and Picture 5-10 for stroke ratio $R = 1$

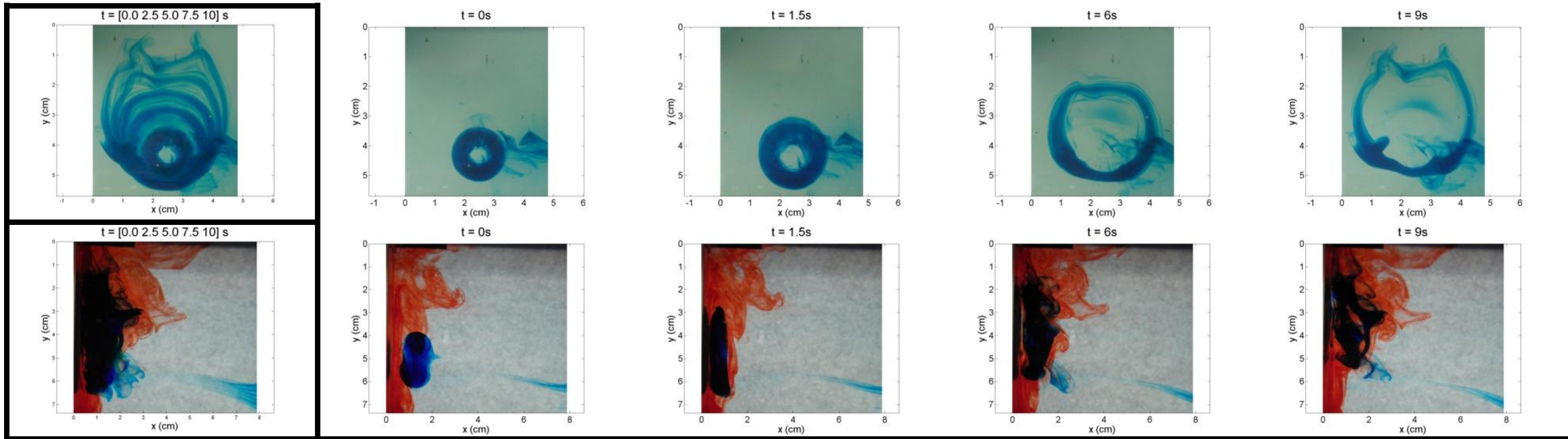

Picture 5-9 Ink visualizations $\Delta T = 35, R = 1$

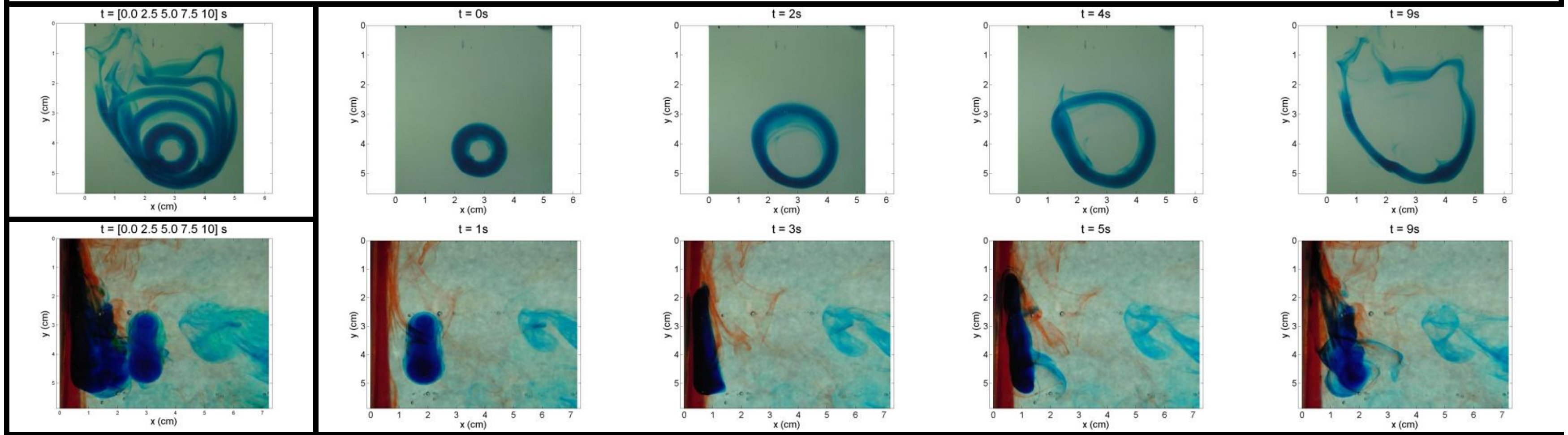

Picture 5-10 Ink visualizations $\Delta T = 50, R = 1$

Finally ink visualizations are performed for Stroke ratio $R = 2$ and a temperature difference. Results are presented in Picture 5-11

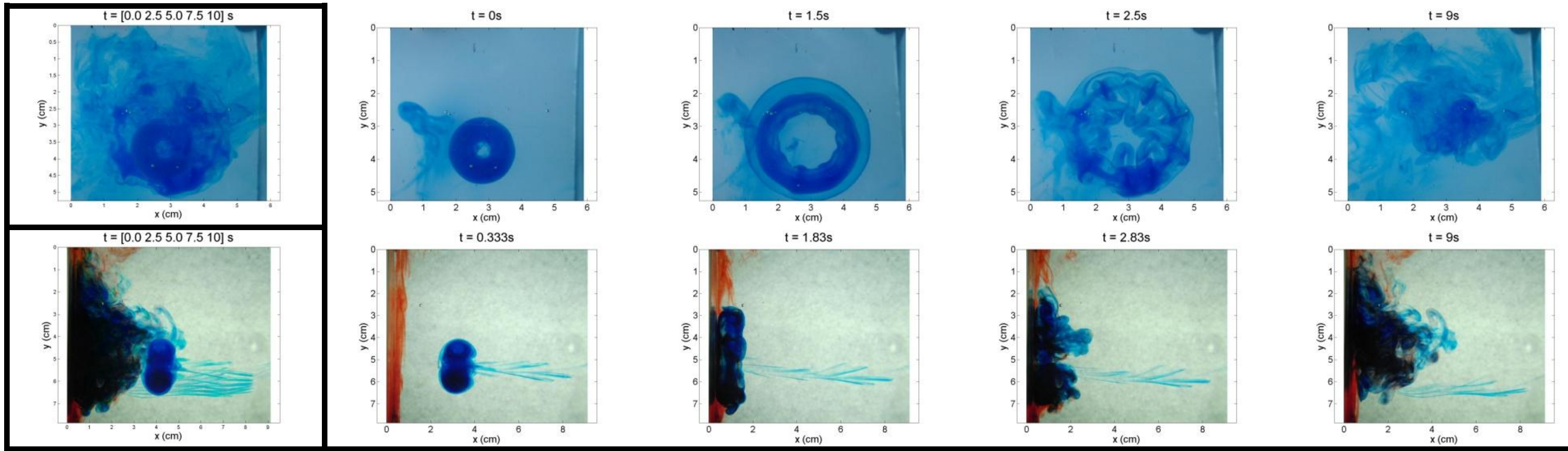

Picture 5-11 $\Delta T = 50, R = 2$

5.3 Schematic description of collision behavior

Looking at the isothermal case, the behavior for stroke ratio 1 and 2 is quite different. For $R = 1$, no boundary layer separation occurs. The vortex ring increases. This is limited by the weakening of the vortex due to dissipation and vortex stretching.

For $R = 2$, boundary layer separation occurs. The newly produced ring moves around the primary ring and wants to move into and through the central hole of the primary ring. Because this doesn't fit a longitudinal geometrical instability occurs, which leads to breakup and reconnection. The new formed vortex rings collide in the center, which results in a turbulent mess.

To make a start with understanding the case with a temperature, it is convenient to look at different parts of the vortex ring separately. This breakup into regions is visualized in Picture 5-12 to Picture 5-14

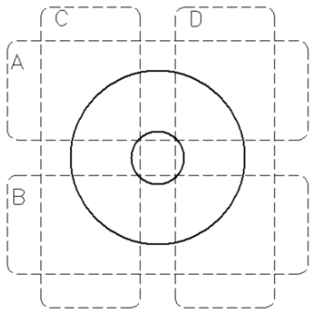

Picture 5-12 Vortex regions

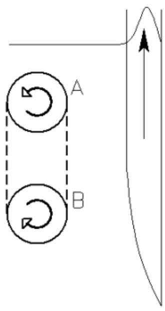

Picture 5-13 Horizontal regions

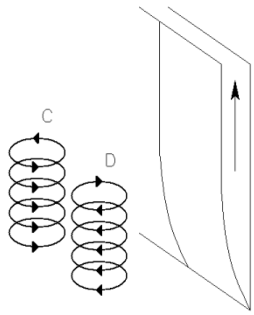

Picture 5-14 Vertical regions

The vortex ring can (in a simplified representation) be divided in 4 parts. The top part has a velocity at the wall-side in a direction which is equal to the convection. The bottom part has a velocity at the wall-side in a direction opposite to the convection. The two side parts have velocities at the wall side which are perpendicular to the convection.

5.4 Vorticity transport

It is beyond the scope of this research to study in detail the vorticity transport. Generally it can be stated that the vorticity transport is dominated by vorticity gradient (laminar case) or Reynolds stress (turbulent case) [12]. It is a challenge to determine the Reynolds stresses for this specific case, but intuitively it would be expected that the maximum vorticity transport is at the place interface between the bottom part of the vortex and the shear flow induced by the convection.

Though, from the experiments we know that the bottom part keeps the vorticity, while the top part loses the vorticity. This can be understood by looking at the vorticity gradient. An example for the situation for $R = 1, T = 70$ is presented in Picture 5-15 to Picture 5-20. It appears that the vorticity gradient at the interface between vortex and convective shear flow is higher for the top part. Viscous dissipation is dependent on the vorticity gradient. Some different reasons can be thought of to explain this phenomenon:

1. Due to the opposite direction of the velocity for the bottom part, the boundary layer velocity decreases locally, which means that the vorticity induced by the boundary layer is low, and as a result the effect on the vortex as well.
2. The distance between the maximum speed of the boundary layer and the center of the vortex is higher for the lower part.
3. Vortex stretching means local decrease in vorticity. The vortex stretches more at the top than at the bottom, which means that the local vorticity decreases more.

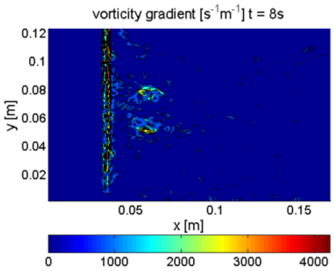

Picture 5-15 Vorticity gradient

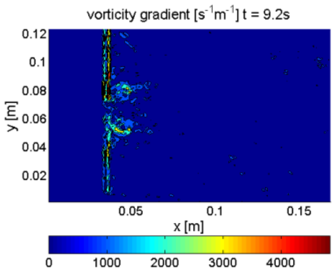

Picture 5-16

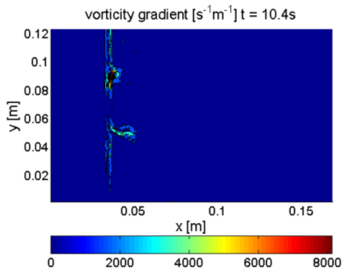

Picture 5-17

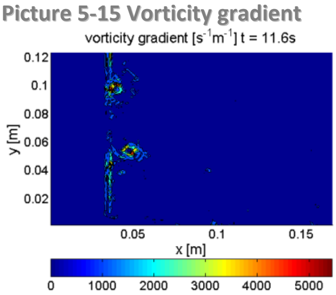

Picture 5-18

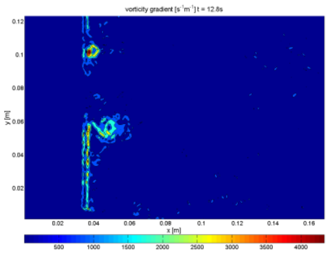

Picture 5-19

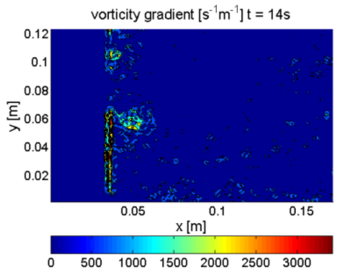

Picture 5-20

5.5 Vortex trajectory

Stroke ratio 1

First the case stroke ratio $R = 1$ is considered. The behavior is generic and reproducible; first the ring diameter increases. On top of that the center of the ring appears to move upward due to convection. After a while the vertical part of the ring appears to move upward faster than the horizontal part, leading to a ‘cat-head’ shape of the ring. At the ‘corners’ left and right of the bottom horizontal part of the ring, an agglomeration of ink appears.

The top and bottom part are easiest to understand. For the force at the vortex center, the convection can be considered as a strengthening (top) or weakening (bottom) of the effect of the ‘mirror vortex behind the wall’ (see chapter 0 on the 2D potential flow model). This causes the top part to move upward even faster, and the bottom part to move downward slower.

The influence of the convection layer to the two vertical parts is in the form of the generation of coaxial swirl. From the ink experiments we see that at the sides the ring moves upward even faster than the top side of the vortex. On top of that we see an agglomeration of ink at the bottom left and right ‘corners’ of the ring.

The fast motion in upward direction of course caused by the boundary layer, but it is strange that it moves even faster than the top region of the vortex ring. Two proposed reasons for this phenomenon are listed below, but further research is required.

1. The boundary layer doesn’t apply a force to the vortex in the direction perpendicular to the wall, as it does for the top part. This might cause the side parts to upwards faster with convection.
2. It should be studied whether the streamlines are still closed for the whole domain. What the ink experiments show is the position of ink, but it is questionable whether this is still the position of the vortex.

Stroke ratio 2

For the stroke ratio $R = 2$ less influence from the convection to the behavior can be observed. Generally it can be stated that the ‘sequence of events’ is too fast. The behavior is not significantly influenced up to the point where the ink is spread to a wide turbulent cloud, and then the cloud convects away.

Further research might be of interest to quantify the influence of the convective shear flow to the collision for variations of dimensionless numbers like dimensionless speed $\frac{v_{convection}}{v_{ring\ propagation}}$, dimensionless circulation $\frac{\Gamma_{convection}}{\Gamma_{ringvortex}}$, dimensionless boundary width $\frac{d_{boundary\ layer}}{r_{ringvortex}}$ and combinations.

6 Quantitative collision characteristics

On top of the ink visualizations also PIV-measurements were performed for the collision of a vortex-ring with a heated wall. These 2D measurements were performed in a 2D plane through the ring-central axis. Unfortunately something went wrong with the vortex-formation, it's still unknown what happened. As a result some of the vortex rings didn't move straight but were bending or followed an oblique path. Because of this reason just individual examples are given for trajectories and circulation.

6.1 Trajectories

First the isothermal case is considered. The behavior expected from the ink-experiments and literature can be observed. The isothermal case is analysed for just a voltage of 60V and a stroke ratio of 1. Other experiments were performed, but with different PIV equipment. This data is available but not yet analyzed.

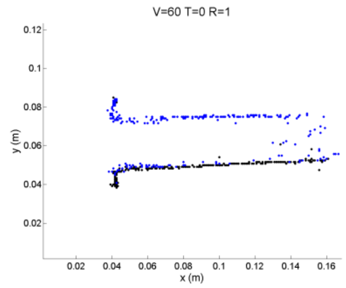

Picture 6-1 Isothermal Trajectory

When the wall is heated, it can be observed in Picture 6-2 that the top vortex indeed moves upward. The vortex at the bottom makes a u-shaped trajectory. First the vortex moves downward, than it moves away from the wall.

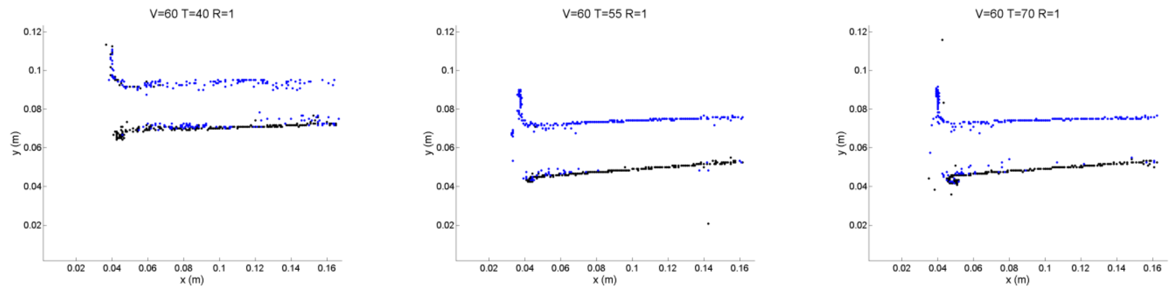

Picture 6-2 Vortex-ring trajectories for different temperatures

Picture 6-3 shows the influence of vortex velocity (through the voltage) on the trajectory. It is not possible to notice relevant differences from this pictures. What is remarkable is the bad tracking of the 20V case. This is caused by the fact that the value Q-criterion here is even lower than the value at the vortices. It is possible to track this vortices better, but this is not yet performed.

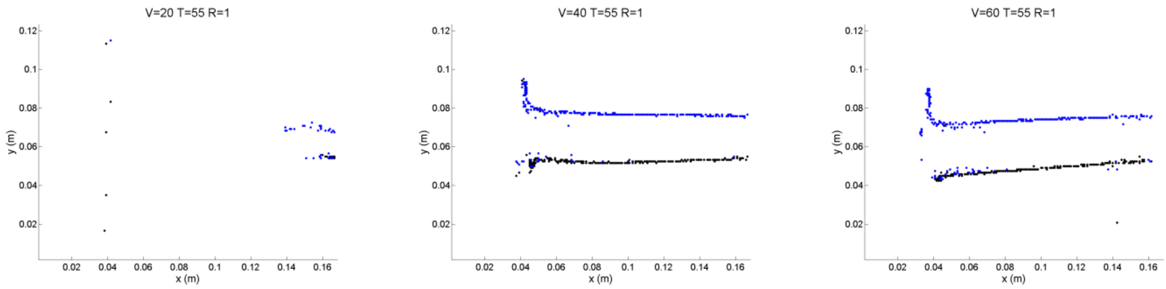

Picture 6-3 Vortex-ring trajectories for different voltages

Finally the influence of stroke ratio is investigated. As expected, for higher stroke ratio's the trajectories of primary and secondary vortices can be found. For the case where boundary layer separation occurs, it appears that after a while a vortex pair (in 3D probably a ring) moves away from the wall in upward right direction.

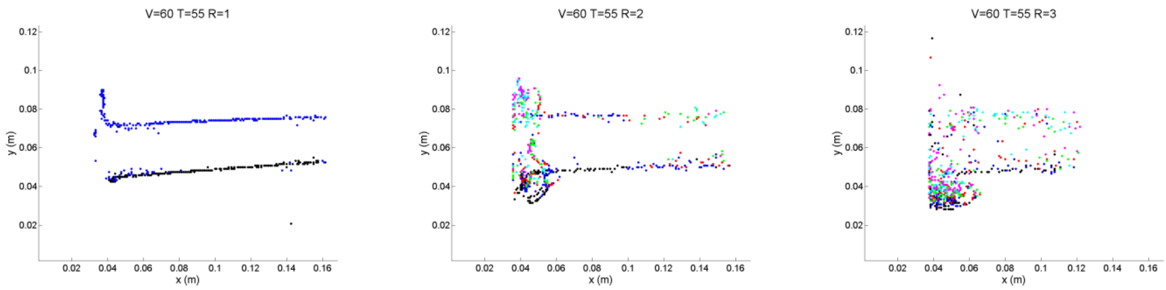

Picture 6-4 Vortex-ring trajectories for different Stroke-Ratios

Schematically, the trajectories are presented below. For R=1, no boundary layer separation occurs. For R=2 or higher, boundary layer occurs, once or more times. After some time a new formed vortex pair moves back in upward direction.

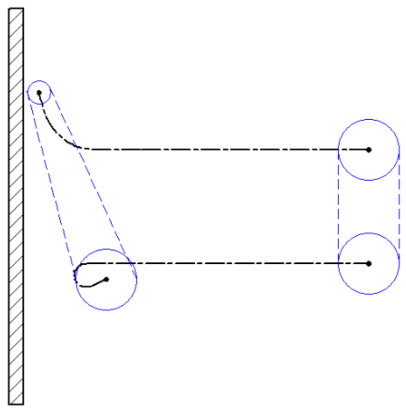

Picture 6-5 Schematic trajectory for $R = 1$

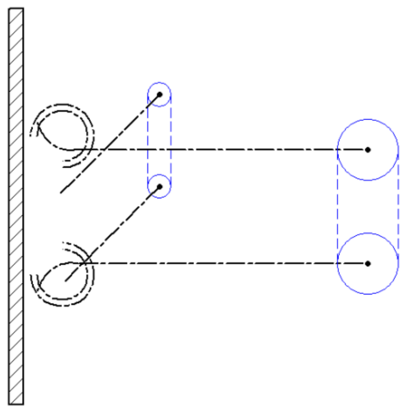

Picture 6-6 Schematic trajectory for $R > 1$

6.2 Circulation

First the isothermal case is considered. The pictures show symmetrical behavior for the top and the bottom part of the domain. The difference in peak-time is caused by a difference in timing. The difference in height of the peak gives an indication of the error present between two experiments. In Picture 6-7 the first graph the 'absolute circulation' is presented, which shows a sudden change in the slope. Before this point the vortex is in free motion, and the change indicates the collision. This graph shows the increase in dissipation after collision.

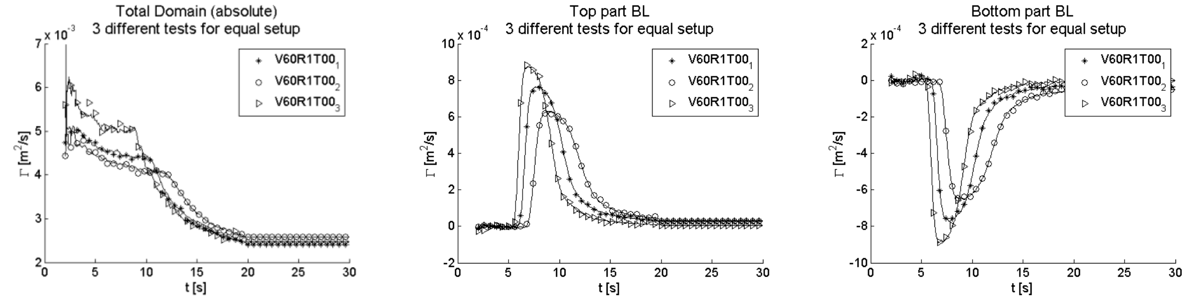

Picture 6-7 Circulation development for Isothermal conditions and $R = 1$

Next the influence of temperature is studied in Picture 6-8. In these cases it seems that a higher temperature gives a higher vorticity, which is shown with the different initial values for 'absolute circulation' in the boundary layer region. For the $T = 70°C$ case it is found that the vortex ring disturbs the boundary layer in such a way that the absolute circulation is even lower for some time after the collision, and then increases again when the boundary layer restores. For the top part, the influence of the collision dissipates slower than for the bottom part. It might be the case that the bottom part of the ring enters the top part, which would be an explanation of this phenomenon. From the development of the (not-absolute) circulation we don't find a trend in positive or negative direction, which indicates that not specific the negative or positive vortex dissipates faster than the other one.

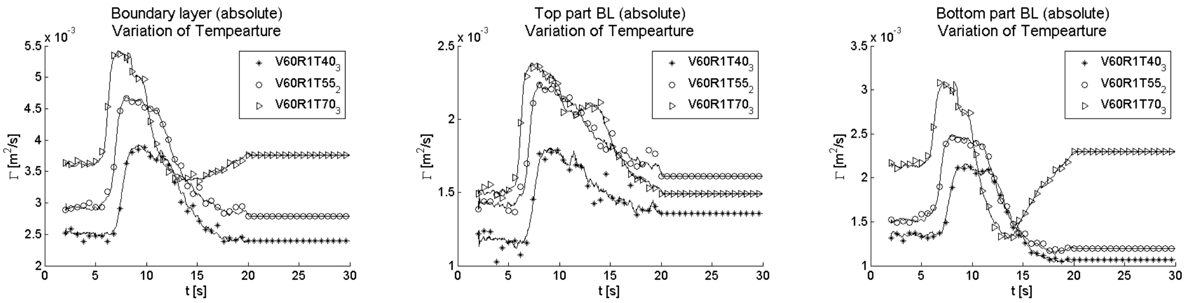

Picture 6-8 Circulation development for different temperatures

Now the influence of impulse, realized using different voltages is presented in Picture 6-9. Each experiment is performed for $T = 55°C$. The $20\ V$case had a delay of 8 seconds, otherwise the vortex-ring wouldn't even have reached the wall yet. Of course it can be noticed that the circulation at start is higher for a higher impulse. On top of that it seems that the vortex for $V = 20$ seems to dissipate slower than vortices which contain more circulation.

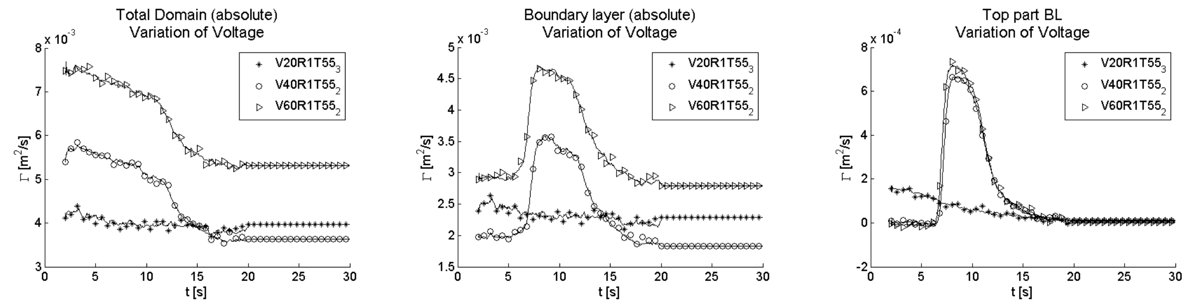

Picture 6-9 Circulation development for different voltages

Finally the influence of stroke ratio is studied. The results are shown in Picture 6-10. From the ink experiments it is already known that the behavior for other stroke ratio's is totally different. As expected, for a higher stroke ratio the initial circulation is higher. In the boundary layer we don't find a reproducible trend which would indicate specific difference in dissipation for the top or bottom vortex. From the absolute circulation for the boundary layer we find that the dissipation goes slower for the $R = 1$ case, which is also expected.

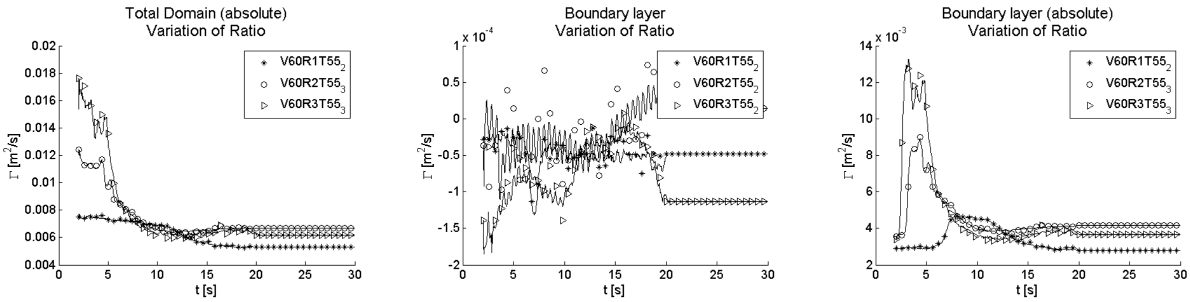

Picture 6-10 Circulation development for different Stroke Ratio's

Appendices

A1 LITERATURE LIST

Scientific references

[1] The impact of a vortex ring on a wall. *Walker, J.D.A., Smith, C.R., Cerra, A.W., Doligalski, T.L.* (1986)

[2] Vortex interactions with Walls. *Doligalski, T.L., Smith, C.R., Walker, J.D.A.* (1994)

[3] Vortex-body interactions. *Rockwell, D.* (1998)

[4] Unsteady heat transfer analysis of an impinging jet. *Chung, Y.M., Luo, K.H.* (2002)

[5] Vortex ring head-on collision with a heated wall. *Arévalo, G., Hernândez, R.H., Nicot, C., Plaza, F.* (2007)

[6] Heat transfer resulting from the interaction of a vortex pair with a heated wall. *Martin, R., Zenit, R.* (2008)

[7] Particle image velocimetry measurements of vortex rings head-on collision with a heated vertical plate. *Arévalo, G., Hernândez, R.H., Nicot, C., Plaza, F.* (2010)

[8] Influence of approach flow conditions on heat transfer behind vortex generators. *Henze, M., Von Wolfersdorf, J.* (2010)

[9] Numerical study of a vortex ring impacting a flat wall. Cheng, M., Lou, J. Luo, L.S.

[10] Vortex Rings (book). *Akhmetov, D.* (2009)

[11] An objective definition of a vortex, *Haller G.* (2005)

[12] Reynolds stress and the physics of turbulent momentum transport, *Bernard, P.S., Handler, R.A.* (1990)

Website references

[A] The World Factbook, *CIA*, retrieved April and October 2012 from https://www.cia.gov/library/publications/the-world-factbook/geos/mx.html

[B] Mexico Economy Profile, *Economywatch,* retrieved April 2012 from http://www.economywatch.com/world_economy/mexico/

A2 RECOMMENDATIONS

Practical

a1. For the ink experiments, it is difficult to obtain the size of the ring and compare between different experiments. An easy method to have an indication of the size is to draw a square to the wall of the basin and the heated wall. This square can be used to obtain dimensions.
a2. The effects of different temperature were negligible for this range of temperatures. A method should be found to increase the range. The easiest improvement is to make the wall from tempered glass instead of acrylic glass.
a3. The bath appeared to be too small. This was strikingly visible doing the ink experiments, where it was visible that the 'cloud' of ink often moved back into the basin, even through the trajectory of the vortex.

Scientific value

b1. To identify quantitative dependency to temperature, just measuring the temperature before adding the wall to the bath is not sufficient. To really study the temperature at the moment of the experiment, it is necessary to make a full numerical model of the boundary layer development using Boussinesq approximation, and compare this to the results.
b2. When proper measurements are obtained without generating a vortex, but for exact the same conditions, the real effect of the vortex ring can easily be found extracting the two datasets. This is possible most specific for integral quantities like circulation, but also for other quantities like velocities of the fluid near the heated wall.
b3. The effect of swirl in the vertical part of the vortex is not yet fully understood. Probably in literature it is possible to find relevant references.
b4. PIV-measurements in a perpendicular vertical plane and a horizontal plane are necessary to understand the 3D behavior of the ring. From the ink-experiments it is impossible to distinguish vorticity transport and just mass transport through the vortex, which is an important difference.
b5. The rate of viscous dissipation is just quantitatively investigated, but not yet qualitatively understood. Based on relations for vorticity transport or Kolmogorov's principles, it should be possible to find a more thorough qualitative explanation of the principles.
b6. The Q-criterion used to determine the vortex is a very basic method, which appeared to be insufficient for weaker vortices (20V case). Improved criteria should be applied to determine the vortices. This is also relevant for the situation after collision. Using the Q-criterion it was not possible to distinguish vorticity related to the primary or the secondary vortex. When a method is found to do this, proper assignment of circulation can be performed, and loss of circulation (due to stretching or dissipation) can be studied in more detail.

A3 SUMMARIES, EMPHASIZING RELEVANT CONCEPTS AND CONCLUSIONS

Personal note: I didn't manage to write a proper literature review within the time set for my internship. I made a start with a thematic overview, which was unfortunately lost when my computer crashed. Though, I still have summaries from some of the articles, and I just attach them in this appendix.

A summary of selected articles is presented in this appendix. The relevant literature is divided in three different categories: vortex rings (VR), vortex interactions with bodies (VIB) and Heat transfer (HT).

The impact of a vortex ring on a wall. Walker, J.D.A., Smith, C.R., Cerra, A.W., Doligalski, T.L. (1986)	VR, VIB
Vortex interactions with Walls. Doligalski, T.L., Smith, C.R., Walker, J.D.A. (1994)	VIB
Vortex-body interactions. Rockwell, D. (1998)	VIB
Unsteady heat transfer analysis of an impinging jet. Chung, Y.M., Luo, K.H. (2002)	HT
Vortex ring head-on collision with a heated wall. Arévalo, G., Hernândez, R.H., Nicot, C., Plaza, F. (2007)	VR, VIB, HT
Heat transfer resulting from the interaction of a vortex pair with a heated wall. Martin, R., Zenit, R. (2008)	VR, VIB, HT
Particle image velocimetry measurements of vortex rings head-on collision with a heated vertical plate. Arévalo, G., Hernândez, R.H., Nicot, C., Plaza, F. (2010)	VR, VIB, HT

Table 3-1 Classification of articles

A 3.1 The impact of a vortex ring on a wall. Walker, J.D., Smith, C.R., Cerra, A.W., Doligalski, T.L. (1986)

This article deals with a vortex-ring approaching a horizontal plane wall, and most specific the flow induced by this event near the wall. This is investigated in an incompressible fluid which is otherwise stagnant. Visualisation is realized by dye injection both to the vortex ring and plane-injection close to the wall. Numerical simulations are applied to study the unsteady boundary layer-flow developing on the wall.

Based on Helmholtz theory on circular rings, a streamfunction for a vortex-ring approaching a wall can be defined. Because the vortex ring approaches his own image, it is clear that the vortex-ring will slow down and because of the forming of a vortex-pair with its image, the ring radius will increase.

First a so-called Kelvin-Hicks ring is considered, using inviscid conditions, where the fluid in the ring is in a state of solid-body rotation. The trajectory for such a ring includes a constant radius far from the wall, and an unbounded growth of the radius near the wall. Because the vortex-core is of constant volume, the vortex core will in turn approach the wall to infinitesimal distance. In practice this will not happen, due to interaction with an unsteady viscous boundary layer.

The viscous boundary layer flow is governed by continuity and momentum conservation expressed in dimensionless terms. The behavior induced by this layer is discussed later.

The experimental results slow formation of a secondary vortex ring where the vortex interacts with the boundary layer. This event is induced by boundary-layer separation. This vortex ring has lower circulation, and moves around the primary vortex, while his diameter decreases. Eventually, if the primary vortex contains sufficient energy, the event happens again, resulting in a tertiary vortex ring. The event of boundary layer separation and emergence of secondary and tertiary vortices starts for rings with Reynolds number $Re_0 > 250$, where the Reynolds number is defined as $Re_0 = \frac{V_0 D_0}{\nu}$, the V_0 and D_0 in this formula are translational velocity and diameter of the fully developed but undisturbed vortex ring. The secondary vortices also have effect on the trajectory of the primary ring; the widening is bounded and the ring rebounds from the wall (temporarily). When the secondary rings completes its orbit around the primary ring, the decrease in diameter causes wavy instabilities in the azimuthal direction. This means that the flow loses its axial symmetry, resulting in a complex 3D flow pattern. The primary vortex was found not to show any azimuthal instability, even not when triggered by the secondary vortex. This behavior was observed for $460 < Re_0 < 1600$.

For higher Reynolds number, another type of instability was observed; the secondary ring develops it's orbit to the inside of the primary ring, but as soon as the tertiary ring appears on top of the primary ring, the secondary ring rapidly ejects and moves away from the wall.

The boundary-layer separation was investigated numerically. Without mentioning mathematical details, qualitatively a form of boundary layer separation was observed. Little downstream of the core of the primary vortex entering the wall, a recirculating area emerges, which rapidly develops after initialization, while growth is 'peak wise' strongest in direction normal to the wall. When the primary vortex approaches, streamlines are compressed together, or otherwise boundary layer growth occurs at the inside of the secondary vortex. After some time, viscous-inviscid interaction between boundary layer and outer flow occurs, resulting in separation of the secondary eddy from the wall. This secondary vortex ring interacts with the primary ring, resulting in a trajectory around the primary ring, which was observed in previous described experiments.

A 3.2 Vortex-body interactions. *Rockwell, D.* (1998)

This article reviews available knowledge about interactions between vortices and finite bodies, which means that the size of the vortex is at least of the same scale as the body.

Some flow-features emerging in this type of interactions are in common with vortex interactions with infinite walls, like boundary-layer separation. Different is the way the vorticity distribution of the incident vortex is distorted. When the vortex is far enough, the surface loading is just a function of the circulation of the vortex, and to estimate the effect, a rectilinear representation of the vortex can be used. The incident vortex can have orientation in 3 directions, but also can have the form of a Karman vortex street.

When a vortex collides with a sharp edge, the vortex undergoes a distortion, and also highly unsteady secondary (tip) vortices emerge, which develop along the surface of the foil. When the length of the body in the direction of the vortex movement is sufficiently small, intriguing flow patterns emerge, with a high sensibility to asymmetry, and vorticity in both directions, with circulation commensurate to that of the incident vortex. For oscilating bodies, the interaction determines to be highly dependent on the phase of the motion at the moment of incidence.

When a vortex enters a cavity, a corner-vortex impingement occurs. This results in a convection role which spans the total cavity. This large scale vortex exists of several smaller scale vortexes, which start from the corner, and go down along the wall, following the recirculation.

For perpendicular incidence of a vortex with a body, most important physical features encounter displacement of the trajectory due to image effects, generation of a separation zone on the surface of the blade and vortex breakdown (onset near the position of maximum thickness).

For a vortex entering a body in the normal direction, both bending and chopping of the vortex can occur. When the vortex is chopped, either a shock or a rarefaction wave develops in the vortex, which moves away from the body.

A 3.3 Unsteady heat transfer analysis of an impinging jet. *Chung, Y.M., Luo, K.H.* (2002)

This article presents a numerical study of the heat transfer influenced by a confined impinging jet. This is a widely used feature to enhance heat transfer.

For the numerical study, the time-dependent Navier Stokes equations are solved, using constitutive equations for the stress tensor and heat flux vector. For the boundaries, no-slip condition is applied. There is no mean flow through the chamber. A sixth order scheme (Lele) is applied, while at the boundary third and fourth order Runge-Kutta schemes are applied. After the flow and heat transfer developed, the averages of different quantities were token for several periods, in order to 'statistically wipe out' the fluctuating nature of the behavior. For this study the CFL-condition (of $=\Delta t < \sqrt{3}$) was exceeded, but this seemed not to cause problems.

Vortices are formed due to shear with the jet. Those vortices move along the jet to the wall. Interaction with the boundary layer results in secondary vortices near the wall. The temperature close to the wall found to oscillate unsteadily. The frequency of this fluctuation is inversely related to the Reynolds number, while the relative magnitude of the peaks increase with the Reynolds number. For higher Reynolds number, the oscillation becomes less regular, which is caused by non-linear effects.

The Nusselt number (defined as $Nu = \frac{D}{\Delta T}\frac{dT}{dy}$), was calculated and averaged over time, which results in typical bell shapes (Close but not equal to gauss distribution, and showing a secondary peak). The stagnation Nusselt number can be related to the Reynolds number using the following fit: $Nu \sim Re^{0.48}$, which is close to theoretical predictions and other experiments. For higher Reynolds number, the Nusselt-profile becomes less smooth, and the local maxima even splits in two maxima for Re=1000.

The heat transfer also shows highly fluctuating behavior in time, caused by unsteady flow patterns, most specific with the vortex dynamics in the flow. Qualitatively, the fluctuations are induced by primary vortices entering the wall. Around the jet, several 'new primary vortices' are formed, which move along to the wall. The Nusselt number in the stagnation point starts to increase when the vortex comes close to the wall, and decreases again when the vortex moves away from the jet, increasing again when the next primary vortex comes close enough.

A 3.4 Vortex ring head-on collision with a heated wall. *Arévalo, G., Hernândez, R.H., Nicot, C., Plaza, F.* (2007)

This article deals with the experimental investigation of the head-on collision of a vortex ring in air to a heated vertical plate. The vortex ring was creating by pushing a volume of air through a hole (for different diameters). Also different impulses were applied. For the setup an insulated electric heater was used, for which the current could be measured, in order to study the heat transfer fluctuations. The dynamic boundary layer was always laminar, and thePrandtl number $Pr \sim 1$ which means that the dynamic and thermal boundary layer share geometrical characteristics scales.

In terms of flow patterns, the collision shows the following behavior: when the ring enters the wall, both thermal and dynamic boundary layers start to be perturbed, than the hot fluid from the boundary layer starts to penetrate the vortex ring, and finally both the perturbed part of the boundary layer and the remainder of the ring convect upwards with the natural convection, and the stable boundary layer restores. The movement of the top part of the ring convects faster than the bottom half. This can be explained by the direction of vorticity in combination with both mirror-effects and the direction of the convection.

With the impingement of the ring, a significant increase in the power consumption could be observed, this peaks were divided in three stages; a rising time of the power fluctuation (I), the settling time of the power fluctuation (II) and the restore time of the power fluctuation (III). The settling time corresponds to an almost linear decay of the power consumption, related to the period in which the ring convects away. The restore time is related to the period to restore the boundary layers. The maximum increase in power and total dissipated energy for both period I and II appeared to be positive related to the Reynolds number.

A 3.5 Heat transfer resulting from the interaction of a vortex pair with a heated wall. *Martin, R., Zenit, R.* (2008)

Of particular interest for this article is a 2D numerical study of the interaction of a compact vortex-ring with a heated wall. Formation and behavior of these structures is well known, and its properties are easily adjustable.

For description of the fluid motion, conditions based on laminar unsteady incompressible flow are used. These conditions are applied to continuity, time dependent momentum and energy conservation. The vortex is initially described by a hill spherical vortex, the velocity is given by an inviscid irrotational formulation, but this condition adapts as soon as the solver is started to a viscous vortex pair. The impact of temperature on buoyancy is not considered, which practically means that natural convection is not considered.

On the numerical solution, it is just mentioned here that an ADI-method is used, while for every ADI-step, a MUSCL scheme was applied.

The results show for the velocities that a secondary vortex of opposite vorticity is found, which is in coherence with other studies. The wall heat transfer, expressed in dimensionless terms as being the Nusselt number, shows an important increase as soon as the vortex enters the wall. After that the heat transfer decreases again, as soon as the heated lump of fluid enters the wall again. However, along with the heated lump, some fresh fluid is dragged over the wall, resulting in a second increase of heat transfer. This process keeps alternating for a while, the tendency of heat transfer is going down to the equilibrium position along with the dissipation of the vortex.

For the study, different Prandtl numbers and Reynolds numbers were applied. The maximum Nusselt number can be related to the Prandtl and Reynolds number using the following fit:

$Nu_{max} = 4.139 Re^{0.113} \mathrm{Pr}^{0.076}$.

A 3.6 Vortex interactions with Walls. Doligalski, T.L., Smith, C.R., Walker, J.D.A. (1994)

The central topic of this paper is a 2D approximation of the flow-pattern induced by interaction of vortices and walls, and vortex generation due to boundary-layer separation induced by flow over a flat plate.

Many features can be studied by a 2D model of a vortex near a wall. Inviscid theory (Milne-Thomson) predicts a propagation velocity $V_c = U_0 - \frac{\kappa}{2a}$. The vortex can be described at one limiting case by a rectilinear vortex, where the vorticity is tightly concentrated in a small core, another discussed limit is a description where the vorticity is distributed over a finite circular area, outside of which the motion is irrotational. The streamlines which belong to this vortex show a stagnation point in the flow for $\alpha > 0.75$ ($\alpha = V_c/U_0$). For $\alpha < 0.75$, two stagnation points exist at the surface, which bracket a region of counter flow.

At high Reynolds numbers, laminar boundary layers appear to abruptly develop a sharply-focused eruption in regions of adverse pressure gradient, which is called separation. This sharp eruption is found to be caused by the fact that fluid particles close to the wall near the point of zero shear experience an extreme compression in tangential direction, and because of continuity they elongate extremely in the direction normal to the wall.

So combining, a vortex moving along a wall will not only move due to the influence of it image at the non-physical domain, but will also cause the eruption of a secondary (or eventually tertiary) vortex in the region of adverse pressure gradient. Those vortices are observed to have a strength of the same order as the primary vortex, and interact in an inviscid manner with the primary vortex. Degani and Walker found that the emergence of a spiky boundary layer eruption is eventually suppressed by a sufficient high wall speed, because in that case the wall speed dominates the boundary-layer development.

The second half of the paper deals with dynamic stall and 3D interaction, which is not of interest for this research.

A 3.7 Particle image velocimetry measurements of vortex rings head-on collision with a heated vertical plate. *Arévalo, G., Hernândez, R.H., Nicot, C., Plaza, F.* (2010)

In addition to earlier work of the same authors, the study of interaction of a vortex ring in air impinging a vertical heated wall in normal direction is extended with Particle Image Velocimetry (PIV) measurements.

The Grashof number $Gr \sim 10^5$ indicates a fully laminar boundary layer, which was confirmed by measurements. Due to the gradient of the boundary thickness in vertical direction of the wall, there is a strong asymmetry along the top-down axis. The upper part of the boundary is thicker, which causes that the down part of the ring can enter the wall to less distance.

Velocity profiles along radial axis of the vortex ring were compared for free motion and close to the wall. When the ring enters the wall, the velocity in the center drops dramatically, while the velocity around the core increases. This suggests that the vortex core region is responsible for an important part of the shear stress field at the wall.

The initially unperturbed vortex ring becomes unstable during the impingement process for higher Reynolds numbers (at least ~ 400) resulting ultimately in vortical structures around the center of impact. When the heater is on, this effect concentrates on the lower part of the vortex ring, where the vorticity of the boundary layer has the same sign as that of the local field of the vortex ring. The azimuthal instability can be explained by Dazin's geometrical model.

When the heater is on, the boundary layer adds to the amount of circulation, resulting in a certain 'vorticity offset'. For the shear stress it is found that there are two peaks of opposite sign near the vertical position of the cores, which are connected with a linear progress. The absolute height of the peak decreases when using a heated plate, and a residual stress appears along the boundary layer.

The results reinforce the idea that during collision, the ring growth is accompanied by an increased surface of impact, and thus the heat transfer is increased.

A 3.8 Influence of approach flow conditions on heat transfer behind vortex generators, M. Henze, J. von Wolfersdorf (2010)

Vortex promotors are often used to enhance heat-exchange. These This article deals with the influence of tetrahedral vortex generators (VGs) on heat transfer. structures only generate longitudinal vortices in the flow direction in the near wall region. This is advantageous to other vortex promotors in terms of friction losses.

For the experimental setup, vortex promotors of different geometry were placed in a rectangular channel. The temperature field was measured using thermochromic liquid crystals, and the flow field was investigated using PIV techniques. Several parameters were varied. Of specific interest are the VG height expressed as ratio with the hydrodynamic boundary layer, and different Reynolds numbers. Additionally also the influence of turbulence intensity was studied.

A 3.9 Comparison in terms of range of dimensionless numbers between different papers

Some relevant dimensionless numbers and dimensions are compared in Table 3-2. The definition of Reynolds number used here is $Re_0 = \frac{U_v D_v}{\nu}$. Some articles use different definitions, which is indicated.

	Re_{0-}	Re_{0+}	Pr	Gr_+	L/D_-	L/D_+	D_{min}	D_{max}	Fluid
Us	800	4000	6.2937	$0.35 * 10^8$	0.75	3.41	0.0095	0.0381	Water
[1]	< 250	2840	6.2937	–	1	3	0.0198	–	Water
[2]	700	100000	–	–	–	–	–	–	-
[3]	850^a	120000^a	–	–	–	–	–	–	-
[4]	300^a	1000^a	1	–	4^b	10^b	–	–	-
[5]	150^a	1000^a	1	10^5	0.025	0.04	0.013	0.02	Air
[6]	250	1000	$0.7 - 100$	$\Delta T = 45$	0	–	–	–	-
[7]	300^a	500^a	1	10^5	0.05	0.05	–	–	Air

Table 3-2 Comparison of different Domains

a. Other definition of Reynolds number is used
b. Other definition of stroke ratio is used

A4 EQUIPMENT

Al the equipment used is presented in Picture 4-1 to Picture 4-10.

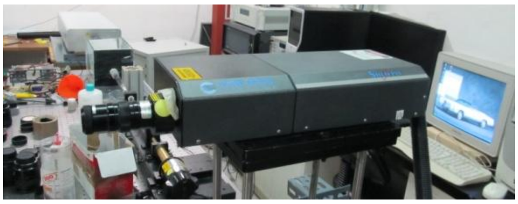
Picture 4-1

Laser 1	
New Wave research	CA 94539
Model	Solo III 15 Hz
Serial number	16046
Voltage	115 V
Current	6 A
Date	November 2000


Picture 4-2

Camera 1	
MegaPlus Camera	
Model	ES 1.0


Picture 4-3

Data buffer	
Dantec	
Model	Flowmap 1500

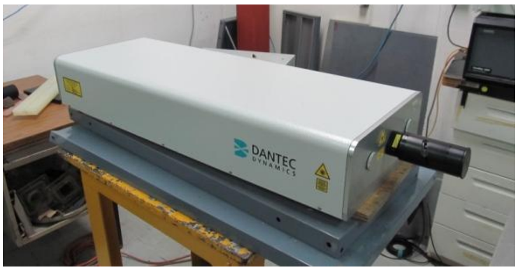

Picture 4-4

Laser 2	
Dantec Dynamics	Litron Lasers
Model no.	LOY201 PiV
Serial no.	LM1146
Voltage	220-250 V @ 50-60 Hz
Current	30 A
Date	December 2010


Picture 4-5

Camera 2	
Dantec Dynamics	
Code	9084C0402
S/N	111
Date	December 2010

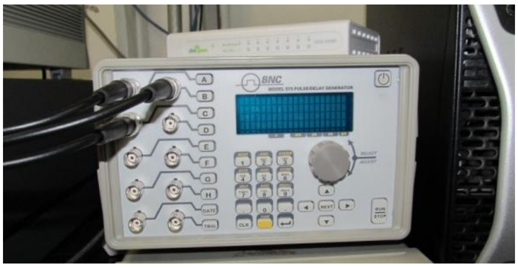
Picture 4-6

Synchronizer	
BNC	Pulse/Delay generator
Model	575

Picture 4-7

Motor	
Baldor industrial motor	
Cat. No.	GP232001
Ser. No.	B010418092
Voltage	90 V DC
Current	0.49 A
Power	1/25 HP
Speed	1720 rpm Cont. Duty (40°C amb.)
Type	2314P
FF	1.35
Frame	FTA-0
Spec. No.	23A006Z002G1
Reducer output:	Reducer output:
Speed	344 RPM
Torque	5.1 LBS. In.
Ratio	5:1

Picture 4-8

Thermal Circulator	
Haake DC10	
Type	003-9774 1200401044017
Voltage	115V/60 Hz
Current	11A
KI: 1DIN12876	IP30

Picture 4-9

Thermal Bath	
Haake K15	
Type	002-4355 1200401029002
Voltage	115 V/60 Hz
Current	14 A
REFR.R134a	IP20

Picture 4-10

Motor Power	
Agilent	System DC Power Supply
Model	6614C
Voltage	0-100V
Current	0-0.5 A

Besides this standard equipment, a vortex generator and a wall were constructed. They are part of the setup, which is presented below.

First in Picture 4-11 a picture is presented of the setup using the first PIV-system.

In the middle the bath is presented with a tube at the left, with a free end in the bath. In this tube you can see the piston. At the right of the bath is a laser, and below, perpendicular to the laser direction a camera is positioned.

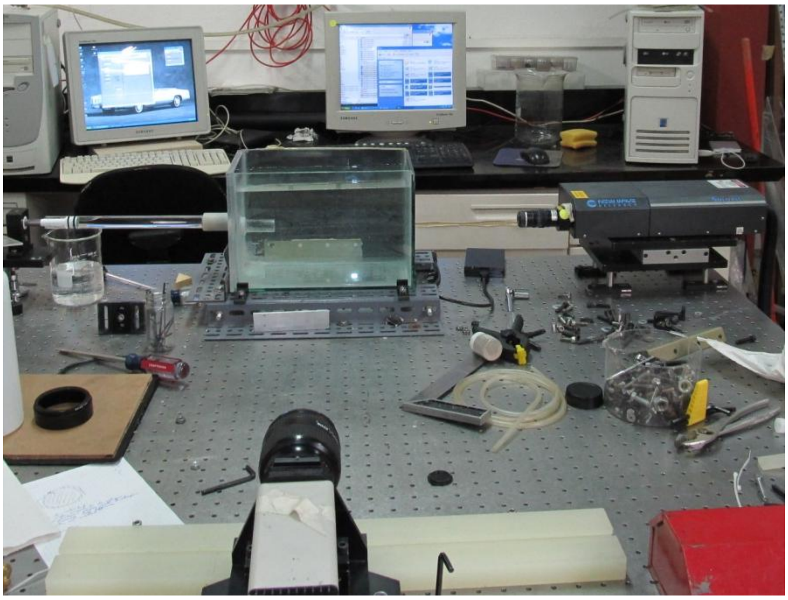

Picture 4-11

In Picture 4-12 the second PIV is applied. This is the reason the bath is placed in opposite direction. At the right of the tube is the sledge, which is connected to the motor at the right. The two computers at the background were for both handling the power supply of the motor and data acquisition. In this figure also the heated wall is placed in the basin.

Picture 4-12

Error! Reference source not found. gives a picture of the wall. The wall is transparent to make it possible for the laser sheet to shine through the wall. At the top a tube is connected for suction and at the bottom for water supply.

Picture 4-13

A5 2D POTENTIAL FLOW MODEL

To study the trajectory of a vortex pair under various conditions, a generic 2D potential flow model was implemented. The mathematical description is given in this appendix.

A 5.1 Geometrical description of a pair of potential line vortices

Location top vortex: $z = z_\Gamma = x_\Gamma + iy_\Gamma = re^{i\theta}, y_\Gamma > 0$

Location bottom vortex: $\bar{z}_\Gamma = x_\Gamma - iy_\Gamma$

Velocity using definition of potential line vortex

For a given associated circulation Γ: $v_\theta = \frac{\Gamma}{2\pi r}$

$u = -\frac{\Gamma}{2\pi r}\sin(\theta), v = \frac{\Gamma}{2\pi r}\cos(\theta)$

Going to a complex representation:

$$u - iv = -\frac{\Gamma}{2\pi r}(\sin(\theta) + i\cos(\theta)) = -\frac{1}{i}\frac{\Gamma}{2\pi r}(-\cos(\theta) + i\sin(\theta)) = \frac{\Gamma}{2\pi i r}e^{-i\theta} = \frac{\Gamma}{2\pi i z}$$

Integrate to obtain the complex potential

$\chi(z) = \int \frac{\Gamma}{2\pi i z}dz = \frac{\Gamma}{2\pi i}\ln\left(\frac{z}{C}\right) = \frac{\Gamma}{2\pi i}\ln(z)$ (choosing $C = 1$)

A 5.2 Equal strength

Complex potential of vortex pair for thin vortices of equal strength located at z_Γ and $\bar{z}_\Gamma$, which means they have the same x-position and an equal distance to the y-axis (which is the center-line)

$$\chi(z) = \frac{\Gamma}{2\pi i}\ln(z - z_\Gamma) - \frac{\Gamma}{2\pi i}\ln(z - \bar{z}_\Gamma)$$

The velocity field of this vortex pair is given by

$$u - iv = \frac{d\chi}{dz} = \frac{\Gamma}{2\pi i}\left(\frac{1}{z - z_\Gamma} - \frac{1}{z - \bar{z}_\Gamma}\right)$$

$$u - iv = \frac{\Gamma}{2\pi i}\left(\frac{1}{x + iy - x_\Gamma - iy_\Gamma} - \frac{1}{x + iy - x_\Gamma + iy_\Gamma}\right)$$

$$= \frac{\Gamma}{2\pi i}\left(\frac{1}{x - x_\Gamma + iy - iy_\Gamma}\frac{x - x_\Gamma - iy + iy_\Gamma}{x - x_\Gamma - iy + iy_\Gamma} - \frac{1}{x - x_\Gamma + iy + iy_\Gamma}\frac{x - x_\Gamma - iy - iy_\Gamma}{x - x_\Gamma - iy - iy_\Gamma}\right)$$

$$= \frac{\Gamma}{2\pi i}\left(\frac{x - x_\Gamma - iy + iy_\Gamma}{(x - x_\Gamma)^2 + (y - y_\Gamma)^2} - \frac{x - x_\Gamma - iy - iy_\Gamma}{(x - x_\Gamma)^2 + (y + y_\Gamma)^2}\right)$$

$$= -\frac{\Gamma}{2\pi}\left(\frac{i(x - x_\Gamma) + (y - y_\Gamma)}{(x - x_\Gamma)^2 + (y - y_\Gamma)^2} - \frac{i(x - x_\Gamma) + (y + y_\Gamma)}{(x - x_\Gamma)^2 + (y + y_\Gamma)^2}\right)$$

So splitting gives:

$$u = -\frac{\Gamma}{2\pi}\left(\frac{(y-y_\Gamma)}{(x-x_\Gamma)^2+(y-y_\Gamma)^2} - \frac{(y+y_\Gamma)}{(x-x_\Gamma)^2+(y+y_\Gamma)^2}\right)$$

$$v = -\frac{\Gamma}{2\pi}\left(\frac{(x-x_\Gamma)}{(x-x_\Gamma)^2+(y-y_\Gamma)^2} - \frac{(x-x_\Gamma)}{(x-x_\Gamma)^2+(y+y_\Gamma)^2}\right)$$

The vortex velocity can be determined for $y \to y_\Gamma$ or $y \to -y_\Gamma$

$$u = -\frac{\Gamma}{2\pi}\frac{2y_\Gamma}{4{y_\Gamma}^2} = \frac{\Gamma}{4\pi y_\Gamma}$$

In order to find the force exerted to the vortex, apply Blasius theorem:

$$F_x - iF_y = i\rho_\infty \oint_C \left(\frac{d\chi}{\mathrm{dz}}\right)^2 \mathrm{dz}$$

$$\frac{d\chi}{dz} = \frac{\Gamma}{2\pi i}\left(\frac{1}{(z-z_\Gamma)} - \frac{1}{(z-\bar{z}_\Gamma)}\right)$$

$$\left(\frac{d\chi}{dz}\right)^2 = -\frac{\Gamma^2}{4\pi^2}\left(\frac{1}{(z-z_\Gamma)^2} - \frac{2}{(z-z_\Gamma)(z-\bar{z}_\Gamma)} + \frac{1}{(z-\bar{z}_\Gamma)^2}\right)$$

The integral now can be solved using the residual theorem, for the upper vortex $z = z_\Gamma$ this gives

$\left(\frac{d\chi}{dz}\right)^2$	*Poles*	*N*	$F(z)$	$\frac{d^{n-1}F}{dz^{n-1}}(z_{pole})$	$\oint_C \left(\frac{d\chi}{\mathrm{dz}}\right)^2 \mathrm{dz}$
$\frac{1}{(z-z_\Gamma)^2}$	$z = z_\Gamma$	2	1	0	-
$-\frac{2}{(z-z_\Gamma)(z-\bar{z}_\Gamma)}$	$z = z_\Gamma$	1	$-\frac{2}{(z-\bar{z}_\Gamma)}$	$-\frac{2}{(z-\bar{z}_\Gamma)}$	$-\frac{2\pi}{y_\Gamma}$
$\frac{1}{(z-\bar{z}_\Gamma)^2}$	-	-	-	-	-

In case the vortex is not free to move, the vortex experiences a force:

$$F_x - iF_y = -i\rho_\infty \frac{2\pi}{y_\Gamma}$$

$$F_x = 0$$

$$F_y = -\rho_\infty \frac{2\pi}{y_\Gamma}$$

A 5.3 Different strength

Complex potential of vortex pair for thin vortices of different strength located at z_1 and z_2

$$\chi(z) = \frac{\Gamma_1}{2\pi i}\ln(z-z_1) + \frac{\Gamma_2}{2\pi i}\ln(z-z_2)$$

The velocity field of this vortex pair is given by

$$u - iv = \frac{d\chi}{dz} = \frac{1}{2\pi i}\left(\frac{\Gamma_1}{z-z_1} + \frac{\Gamma_2}{z-z_2}\right)$$

$$u - iv = \frac{1}{2\pi i}\left(\frac{\Gamma_1}{x + iy - x_1 - iy_1} + \frac{\Gamma_2}{x + iy - x_2 - iy_2}\right)$$

$$= \frac{1}{2\pi i}\left(\frac{\Gamma_1}{x - x_1 + iy - iy_1}\frac{x - x_1 - i(y - y_1)}{x - x_1 - iy + iy_1} + \frac{\Gamma_2}{x - x_2 + iy - iy_2}\frac{x - x_2 - i(y - y_2)}{x - x_2 - iy + iy_2}\right)$$

$$= \frac{1}{2\pi i}\left(\Gamma_1\frac{x - x_1 - i(y - y_1)}{(x - x_1)^2 + (y - y_1)^2} + \Gamma_2\frac{x - x_2 - i(y - y_2)}{(x - x_2)^2 + (y - y_2)^2}\right)$$

$$= -\frac{1}{2\pi}\left(\Gamma_1\frac{i(x - x_1) + (y - y_1)}{(x - x_1)^2 + (y - y_1)^2} + \Gamma_2\frac{i(x - x_2) + (y - y_2)}{(x - x_2)^2 + (y - y_2)^2}\right)$$

So splitting gives:

$$u = -\frac{1}{2\pi}\left(\frac{\Gamma_1(y - y_1)}{(x - x_1)^2 + (y - y_1)^2} + \frac{\Gamma_2(y - y_2)}{(x - x_2)^2 + (y - y_2)^2}\right)$$

$$v = -\frac{1}{2\pi}\left(\frac{\Gamma_1(x - x_1)}{(x - x_1)^2 + (y - y_1)^2} + \frac{\Gamma_2(x - x_2)}{(x - x_2)^2 + (y - y_2)^2}\right)$$

The vortex velocity can be determined for $x \to x_1 \,\&\, y \to y_1$ or $x \to x_2 \,\&\, y \to y_2$

$$u_1 = -\frac{\Gamma_2}{2\pi}\frac{y_1 - y_2}{(x_1 - x_2)^2 + (y_1 - y_2)^2}$$

$$u_2 = -\frac{\Gamma_1}{2\pi}\frac{y_2 - y_1}{(x_2 - x_1)^2 + (y_2 - y_1)^2}$$

$$v_1 = \frac{\Gamma_2}{2\pi}\frac{(x_1 - x_2)}{(x_1 - x_2)^2 + (y_1 - y_2)^2}$$

$$v_2 = \frac{\Gamma_1}{2\pi}\frac{(x_2 - x_1)}{(x_2 - x_1)^2 + (y_2 - y_1)^2}$$

Definitions above mean that the difference in velocity is linearly dependent on the circulation and the weaker vortex moves faster.

A 5.4 Different strength and a wall

Complex potential of vortex pair for thin vortices of different strength but equal x-position located at z_1 and z_2, which are close to a wall which is located (for the generic case) at $y = y_w$. This means that $y_3 = y_1$, $y_4 = y_2$, $x_3 = 2x_w - x_1$ and $x_4 = 2x_w - x_2$

$$\chi(z) = \frac{\Gamma_1}{2\pi i}(\ln(z - z_1) - \ln(z - z_3)) + \frac{\Gamma_2}{2\pi i}(\ln(z - z_2) - \ln(z - z_4))$$

The velocity field of this vortex pair is given by

$$u - iv = \frac{d\chi}{dz} = \frac{1}{2\pi i}\left(\Gamma_1\left(\frac{1}{z - z_1} - \frac{1}{z - z_3}\right) + \Gamma_2\left(\frac{1}{z - z_2} - \frac{1}{z - z_4}\right)\right)$$

$$u - iv = \frac{1}{2\pi i}\left(\Gamma_1\left(\frac{1}{x+iy-x_1-iy_1}-\frac{1}{x+iy-x_3-iy_3}\right)\right.$$
$$\left.+\Gamma_2\left(\frac{1}{x+iy-x_2-iy_2}-\frac{1}{x+iy-x_4-iy_4}\right)\right)$$

$$=\frac{1}{2\pi i}\left(\Gamma_1\left(\frac{1}{x-x_1+iy-iy_1}\frac{x-x_1-iy+iy_1}{x-x_1-iy+iy_1}-\frac{1}{x-x_3+iy-iy_3}\frac{x-x_3-iy+iy_3}{x-x_3-iy+iy_3}\right)+\Gamma_2\ldots\right)$$
$$=\frac{1}{2\pi i}\left(\Gamma_1\left(\frac{x-x_1-iy+iy_1}{(x-x_1)^2+(y-y_1)^2}-\frac{x-x_3-iy+iy_3}{(x-x_3)^2+(y-y_3)^2}\right)+\Gamma_2\ldots\right)$$
$$=-\frac{1}{2\pi}\left(\Gamma_1\left(\frac{i(x-x_1)+(y-y_1)}{(x-x_1)^2+(y-y_1)^2}-\frac{i(x-x_3)+(y-y_3)}{(x-x_3)^2+(y-y_3)^2}\right)+\Gamma_2\ldots\right)$$

So splitting gives:

$$u=-\frac{1}{2\pi}\left(\Gamma_1\left(\frac{(y-y_1)}{(x-x_1)^2+(y-y_1)^2}-\frac{(y-y_3)}{(x-x_3)^2+(y-y_3)^2}\right)+\Gamma_2\ldots\right)$$
$$v=\frac{1}{2\pi}\left(\Gamma_1\left(\frac{(x-x_1)}{(x-x_1)^2+(y-y_1)^2}-\frac{(x-x_3)}{(x-x_3)^2+(y-y_3)^2}\right)+\Gamma_2\ldots\right)$$

The vortex velocity can be determined for $x \to x_1$ & $y \to y_1$ or $x \to x_2$ & $y \to y_2$

$$u_1=-\frac{1}{2\pi}\left(\Gamma_1\frac{y_3-y_1}{(x_1-x_3)^2+(y_1-y_3)^2}\right.$$
$$\left.+\Gamma_2\left(\frac{y_1-y_2}{(x_1-x_2)^2+(y_1-y_2)^2}-\frac{y_1-y_4}{(x_1-x_4)^2+(y_1-y_4)^2}\right)\right)$$

$$u_2=-\frac{1}{2\pi}\left(\Gamma_1\left(\frac{y_2-y_1}{(x_2-x_1)^2+(y_2-y_1)^2}-\frac{y_2-y_3}{(x_2-x_3)^2+(y_2-y_3)^2}\right)\right.$$
$$\left.+\Gamma_2\frac{y_4-y_2}{(x_2-x_4)^2+(y_2-y_4)^2}\right)$$

$$v_1=-\frac{1}{2\pi}\left(\Gamma_1\frac{x_3-x_1}{(x_1-x_3)^2+(y_1-y_3)^2}\right.$$
$$\left.+\Gamma_2\left(\frac{x_1-x_2}{(x_1-x_2)^2+(y_1-y_2)^2}-\frac{x_1-x_4}{(x_1-x_4)^2+(y_1-y_4)^2}\right)\right)$$

$$v_2=-\frac{1}{2\pi}\left(\Gamma_1\left(\frac{x_2-x_1}{(x_2-x_1)^2+(y_2-y_1)^2}-\frac{x_2-x_3}{(x_2-x_3)^2+(y_2-y_3)^2}\right)\right.$$
$$\left.+\Gamma_2\frac{x_4-x_2}{(x_2-x_4)^2+(y_2-y_4)^2}\right)$$

A 5.5 Shear flow

Now finally the same procedure can be used to simulate the shear flow. This operation is not performed here, because the formula’s would be very large. The contribution of each vortex is evaluated in a loop through all vortices used to model the shear flow.

A6 DETERMINATION OF THE VORTEX CENTER

In Paragraph 2.6 the determination of the vortex center is named. In this appendix the background is elucidated.

Curvature

One method to determine the vortex center is to determine the position of maximum curvature. In paragraph 0 it can be found that some additional peaks appear for the vorticity in the areas with low velocity. Those peaks are usually higher than the peak at the center of vorticity. To avoid detecting noisy peaks, the maximum curvature is determined in an area which is selected using the Q-criterion. In Picture 6-1, a surface plot of the curvature field is given, while in Picture 6-2, a surface plot of just the selected area is given.

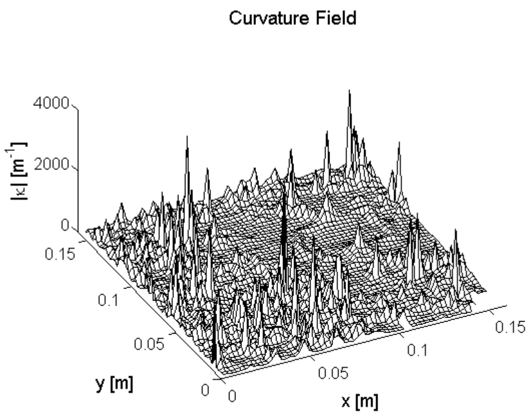

Picture 6-1 Curvature field

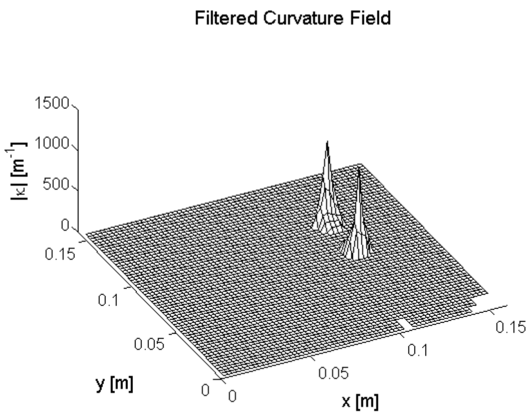

Picture 6-2 Filtered curvature field

Vorticity

An intuitive method to determine the center of the vortex is to use the maximum vorticity. Though, vorticity is a measure of the gradient of velocity in different directions. This means that a shear layer also gives a contribution to vorticity. In the case of a vortex ring, the maximum vorticity tends to be found in between the geometrical center of the vortex and the axis of the vortex ring rather than just at the geometrical center of the vortex. This shift is caused by the influence of the high velocity gradients inside the vortex ring. In Picture 2-5, the maximum vorticity is represented. To avoid this influence, the geometrical center of the vortex can be found by determining the maximum vorticity of the normalized velocity field which is shown in Picture 6-3. The vorticity field of this normalized velocity field is shown in Picture 6-5. For this method, an area should be selected based on the Q-criterion, because very weak fluid motion far from the vortex now gives comparable peaks in the vorticity field.

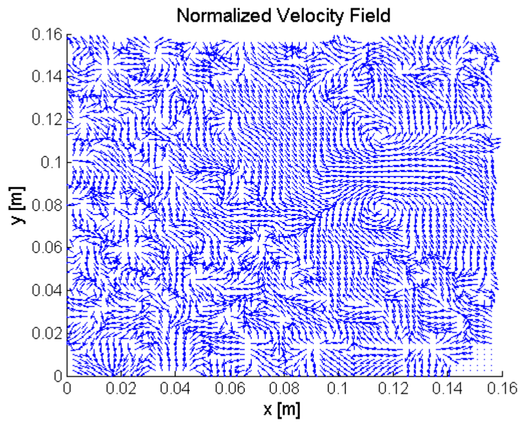

Picture 6-3 Normalized velocity field

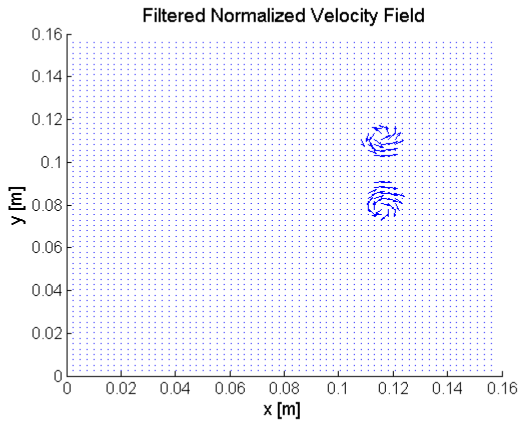

Picture 6-4 Filtered normalized velocity field

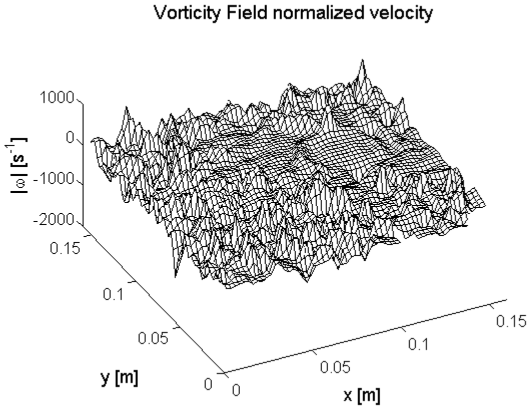

Picture 6-5 Vorticity field normalized velocity

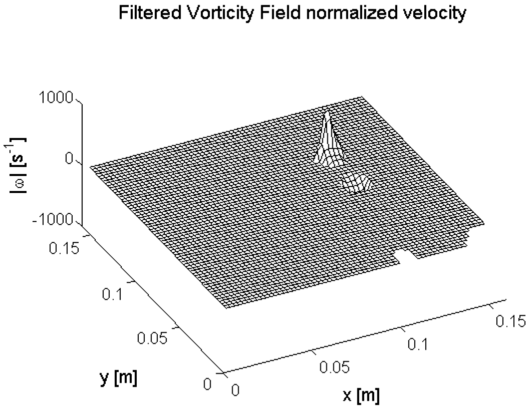

Picture 6-6 Filtered vorticity field

A7 Summary of activities

Because of a computer-crash and lack of suitable backup, my log was lost so I don't have a detailed and thorough overview of my activities during my internship. Instead, I try to recover my activities.

A 7.1 Preparations in Holland

Since two years ago, I started to do some language courses.

From the beginning of the academical year 2011-2012, I started practical preparations of my internship. First I updated my CV, wrote an application letter and translated those to English and Spanish. I studied the requirements for the internship and started to send application letters, and asked different faculties and people for contact details.

After a lot of letters and attempts, I finally found a suitable internship via Prof. Detlef Lohse (Physics of Fluids, UT). After organizing the agreements, I applied for required VISA. Even though most people go to Mexico without VISA, officially I need one for an internship, and I decided to organize it properly.

A 7.2 First weeks in Mexico

Once in Mexico, I still had different opportunities. To make a thorough choice, I read some background information about the different topics, and wrote concise proposals for two projects; one on biological locomotion, one on interaction between ring-vortices and a heated wall. This led to my choice for the ringvortex-project.

Since I made the choice, I read a lot of background information about the general topic of ringvortices, natural convection and interaction of vortices with walls. I made notes, which were later on processed in a kind of literature study.

In the meanwhile, I received some PIV data of moving ring-vortices, and I used this data to get used to processing this kind of data, and to fully understand the steps and difficulties of processing.

A 7.3 Experiments

Once I finished this work, the equipment became ready to use, and we started to do some preliminary experiments. The first aim was just to reproduce earlier results on vortex rings. Later on we started to study the collision between vortex rings and walls. We tried to find optimal settings for the equipment and a proper range of experimental conditions. While doing this we found that this PIV system actually wasn't fast enough to capture the motion we wanted to study, so we switched to another system. Though, this system was quite new, and there were some difficulties to overcome in processing data from this equipment. Once this system was working properly, we did a lot of tests for different conditions using the PIV system.

Because we presumed some asymmetrical behavior (which cannot be catched by PIV measurements because PIV just gives 2D information) we decided to do some ink-visualisations. We injected some dye of one color in the tube where the vortex ring was formed, and some other below the heated wall, so it was convected along the wall. When making a video from the side and the back, the behavior of both the vortex ring and the boundary layer could be visualized.

A 7.4 Report

In the meanwhile, my computer crashed. Even though I could recover most of the files, I had to do some analysis again (fortunate enough the data was stored elsewhere). The most damaged part was unfortunately my report, which means that the process of writing a report was far from ideal. I started writing the new report in the last week before I departed.

Roberto and Charly, my supervisors at UNAM, preferred to see a report in the layout of an article. On top of this, they invited me to help writing an official paper to submit to an influential journal in the field of fluid mechanics or heat transfer. This is not yet finished, and will take another few months of work in spare time.

A 7.5 Supervision

My official supervisor at UNAM was Prof. Roberto Zenit, chair of the group of Rheology. Practically, a lot of work was done in cooperation with, and supervised by Dr. Carlos Palacios, researcher at the same institute. Once every few weeks we had a meeting with three of us to discuss the progress and the planning for the time left. With Carlos I discussed the work on a daily basis.

A8 Country study: Mexico

A summary of some important aspects of the country of destination, Mexico, is presented in this appendix. Most of the data is retrieved from the World factbook [A] and Economywatch [B].

A 8.1 Geographical, natural and environmental information

Mexico is a huge country located at the North American continent, bordering the United States in the north, Belize and Guatemala in the south, the North Pacific Ocean at the west and the Gulf of Mexico and the Caribean sea at the east. The total area of the country is 1,964,375 km2, which means that the country is more than 47 times the size of the Netherlands.

The climate varies from desert to tropical. The desert areas are located at the north, while the tropical area (rainforests) are located in the south. The terrain varies with high rugged mountains, low coastal plains, high plateaus and deserts.

In mexico, often earthquakes and volcano eruptions occur. The country is part of Pacific ring of fire, bordering at the west to the Middle America Trench. The latter causes a risk of tsunamis at the pacific coast. Important volcano's are Colima (last eruption in 2010) and Popocatepetl (last big eruption 2000, also currently active). Both are located in quite densely populated area's, while Popocatepetl is close (80 km) to Mexico city.

The country has to deal with a number of serious environmental hazards. The capital and some other cities at the US border are subject to serious air pollution and smog formation. In the north of the country the deserts increase size rapidly. Many areas have scarce natural fresh water, and population has poor access to clean drinking water. Sewage and industry pollute rivers in urban areas. Other problems are deforestation, erosion, land-subsidence and deteriorating agricultural lands.

A 8.2 Political situation

History

To understand the background and relevance of 2012 political situation in Mexico, some knowledge about the history is required. My experience is that most people in Mexico know a lot of details about their history, and they were willing to tell me about that. A brief summary is given below.

Up to 1521, Mexico was governed by many traditional cultures, the Aztecs and Mayas probably are the most well known examples. Currently this period is often indicated as the pre-Hispanic period. Though, in 1521 Mexico was conquered by the Spanish invaders, which was the beginning of the colonial period, which would last for 300 years. This Spanish conquest is still of important influence in the current culture of Mexico. First of all most Mexicans have Spanish ancestors, but they also still blame the Spanish that they destroyed their culture and killed many people.

Since 1808, a revolution for independence started in Mexico. Miguel Hidalgo y Costilla, a local priest, led the movement against the Spanish suppressors, and on 16 September 1810, he issued the 'Cry of Dolores', an event that marked the beginning of the war on independence, and which ultimately led to the execution of Miguel Hidalgo. In 1821 the Spaniards withdrew, signing the treaty of Cordoba.

The period up to 1976 now is most specific well known for its chaos and insecurity, there was a 2 years war with the United States and more than one president each year was 'worn'. Since 1876 to 1911, Mexico was governed by the dictator Porfirio Díaz, which strictly didn't allow re-elections.

The period 1910 to 1929 is now referred to as the Mexican Revolution. In 1911, finally Porfirio Díaz allowed re-elections. Though, he and his followers very obviously influenced the results, which led to a period of violent disagreements. Finally in 1920 the military Álvaro Obregón became president, and he can be considered as the military winner of the revolution. After 4 years he assigned Plutarco Elías Calles as his successor. During this period Mexico experienced another war, the Cristero war, which was a Catholic counter-movement against the Calles regime. In 1928 Obregón was re-elected, though before his second inauguration he was assassinated by a catholic assassinator.

After new elections, in 1929 a new party won the elections, the New Revolutionary Party, founded by Calles. This party is currently called the Institutional Revolutionary Party (PRI). This party celebrated his success with 71 subsequent years of governing the country. The party was very successful and held responsible for the Mexican Economic Miracle of 1930-1970. After 1970 the economic growth stopped. On top of that they became related more and more to electoral fraud, corruption and relations with drugs cartels. Piece by piece the party collapsed, with a split-up with the left wing of the party in 1986 and the loss of absolute majority in congress in 1997. This finally led in 2000 to the end of the hegemony.

In 2000, the New Action Party (PAN) won the elections, and the transfer of power was quite quick and peaceful. Unfortunately for Vicente Fox, the new president, PAN didn't manage to win a majority in both chambers in congress, which prevented him from implementing his reform pledges.

In 2006, PAN continued to win the new elections, with a very important statement to work on the drugs related violence which afflicted the north of the country. Though, the difference with the runner up was just 0,56%, which is little more than 200.000 votes. Andres Manuel Lopez Obrador, the losing runner up, organized protests which obstructed one of the main roads through the capital for more than a month. The new president, Felipe Calderón, announced the 'war on drugs' in 2006. In 2012, Calderón admitted that the Mexican state was about to lose the war on drugs. More than 50.000 people died due to violence related to drugs since the war on drugs was started.

Elections

During my stay in Mexico, there were new presidential elections. For the 2012 elections, four parties were imposing a candidate for the elections, but in practice only the first three of the list below played a role during elections.

- Enrique Peña Nieto, Current president of Institutional Revolutionary Party (PRI)
- Andrés Manuel Lopez Obrador, Candidate for a coalition led by the Party of Democratic Revolution (PRD)
- Josefina Vázquez Mota, Candidate for the National Action Party (PAN)
- Gabriel Quadri de la Torre, Candidate for the New Alliance Party (PANAL)

As stated before, the most important candidates were from PRI, PRD and PAN.

PAN realized that the lost drugs on war didn't contribute to their popularity. They tried to regain the confidence by imposing a woman candidate. The most important word during the campaign was 'diferente'. They really tried to make sure that the violence wouldn't continue, even when they were re-elected. On top of that, they tried to gain women votes by the feminist appearence of Josefina.

PRI tried to repair the damaged image which was still there due to accusations about electoral fraud. They had the chance because many people were really disappointed in the PAN because of the drugs war. Peña Nieto is a very charming handsome young candidate. He was very popular in the countryside, and, indeed, amongst lower educated young women. We really saw an impression of his popularity during our 2 weeks travel through the country. On the contrary, in the capital city he was the least popular candidate.

PRD participated with the same candidate as last elections in 2006. Andres Manuel Lopez Obrador (often abbreviated to AMLO) lost popularity with the riots he led after the 2006 elections. Though, he is still the socialist candidate and very popular, most specific amongst students and in the capital.

Apart from movements and active campaigns for specific candidates, there was also a movement which was not supporting a specific candidate, but tried to convince of the unreliability of a specific candidate: Enrique Peña Nieto. This (student) movement was called Yo Soy #132. The name originates from a story where Enrique at may 11 2012 came to a private college, the Ibero American University, debating with students. These apparently rich students were expected to be at his hand, though unfortunately they were very critical, strongly expressing their opposition to Peña Nieto. PRI accused them that they were hired by AMLO to blame him at this event. Afterwards, the students made a you-tube video where they all showed their student credentials. Because of the number of students, 131, many students showed their support by writing they were number 132.

Finally the elections were won by the PRI, and Enrique Peña Nieto is the new president of Mexico. But still there are many stories of subornation for votes. AMLO again went to court to fight the outcome and many votes were re-counted. This all didn't make a difference.

A 8.3 Economic situation

The economy of Mexico is the 13th largest economy in the world in nominal Gross Domestic Product (GDP) terms ($1.155 trillion – 2011) and the 12th largest economy in Purchasing Power Parity (PPP) terms ($1.662 trillion – 2011).

The Mexican economy is a free market economy, dominated by the private factor. 62% of GDP is generated by the private factor (34,2% industry, 3,8% agriculture). In labor force the share of services is proportional with 62,9%. (23,4% industries, 13,7% agriculture). Unemployment is officially very low (5,2% - 2011) but underemployment is probably as high as 25%. This is also indicated by the population below poverty line (51,3%, food-based definition – 2010).

Important agricultural products are corn, wheat soybeans and tobacco. Important industries are food and beverages, clothes and textiles, tobacco and also automotive. Around 3 million cars are currently produced in Mexico on yearly basis. Tourism is a growing sector, currently most specific for tourists from the USA.

Since the implementation of the North American Free Trade Agreement (NAFTA) , trades with the USA increased. Currently 71,7% of the Mexican export goes to the USA. Import and export are pretty much balanced with $350,8 billion of imports and 349,7 billion of exports (2011). 62,2% comes from the USA, and 7,5% from China. From the other side Mexico contributes up to 12% of USA imports (7% before NAFTA)

In 2009, Mexican GDP plunged 6,2% as a result of decreasing export demands due to economic crisis around the world. Part of this also might be caused by the outbreak of Mexican-flu.